UNIVERSIDAD TÉCNICA FEDERICO SANTA MARÍA

DEPARTAMENTO DE FÍSICA

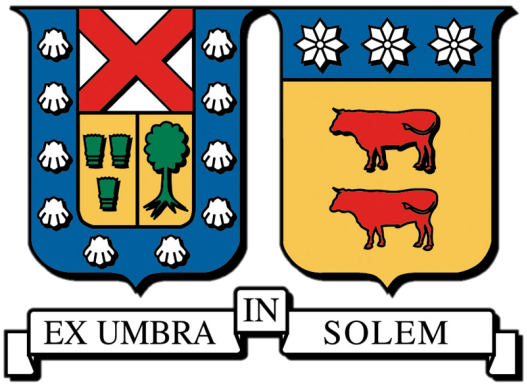

Magnetic field generation in white dwarfs: comparing model predictions with the observations of close double white dwarfs

Sarai Zapata Alarcón

MEMORIA PARA OPTAR AL GRADO MAGÍSTER CIENCIAS, MENCIÓN FISICA

PROFESOR: Matthias Schreiber

March 15, 2024

Resumen

Durante numerosos años, ha persistido la pregunta sobre por qué ciertas enanas blancas poseen campos magnéticos fuertes mientras que otras no. Se han formulado varias teorías para explicar la generación de estos campos magnéticos. El escenario de campo fósil postula que los campos magnéticos observados en enanas blancas se originaron durante las etapas anteriores de las estrellas Ap o Bp. Otra propuesta implica fusiones de núcleos doblemente degenerados, donde la fusión de dos enanas blancas resulta en la creación de campos magnéticos robustos. Una teoría alternativa sugiere que se genera un dínamo durante la fase de envoltura común de un sistema binario. En este escenario, la rotación diferencial en la envoltura común que rodea a las dos estrellas puede impulsar un dínamo, dando lugar al campo magnético de la enana blanca. En la última década, ha surgido una nueva teoría como una explicación posible para los campos magnéticos en enanas blancas. Según esta teoría, el dínamo es impulsado por la cristalización de la enana blanca junto con una rotación rápida.

Tan pronto como una enana blanca de carbono/oxígeno (C/O) está cristalizando, el núcleo sólido se enriquece en oxígeno, mientras que las zonas exteriores ricas en carbono se vuelven convectivas. Esta situación se asemeja a la de la Tierra, en la cual un núcleo de hierro sólido rodeado por una zona de convección líquida junto con la rotación impulsa un dínamo magnético que se supone genera el campo magnético de la Tierra. Basándose en esta analogía, se ha propuesto que un mecanismo de dínamo similar es responsable del desarrollo de campos magnéticos fuertes en enanas blancas.

El objetivo de esta tesis es contrastar dos teorías: una que propone la generación de un dínamo dentro de la envoltura común y la teoría alternativa que sugiere un dínamo impulsado por los procesos de cristalización y rotación rápida. Este trabajo implicará un análisis comparativo con datos observacionales.

Para llevar a cabo este proyecto, se utilizó un código BSE modificado para generar una población significativa de sistemas binarios de enanas blancas cercanas que se formaron a través de dos fases de envoltura común. Posteriormente, se utilizaron ecuaciones proporcionales simples para la fuerza del campo magnético generado por un dínamo dentro de la envoltura común y el dínamo de cristalización para predecir la fracción y las fuerzas de campo de enanas blancas en binarias

dobles cercanas. Al comparar la predicción de nuestro modelo de población con las observaciones de enanas blancas dobles, obtenemos los siguientes resultados.

Primero, dos fases de envoltura común no pueden representar la principal vía de formación para la población actual de enanas blancas dobles observadas, ya que las masas predichas difieren sustancialmente. Para una comprensión completa de la población de enanas blancas dobles en general y de sus campos magnéticos en particular, se requieren modelos de población que incluyan transferencia de masa estable.

En segundo lugar, la teoría del dínamo de envoltura común predice muchas enanas blancas fuertemente magnéticas en comparación con las observaciones, así como una relación entre el período orbital y la fuerza del campo que no se observa. Incluso si solo una pequeña fracción de enanas blancas dobles se forma a través de dos fases de envoltura común, el dínamo de envoltura común en su forma actual no puede describir adecuadamente la generación de campos magnéticos en enanas blancas dobles.

En tercer lugar, las predicciones del dínamo impulsado por la cristalización podrían estar en acuerdo con las observaciones si la eficiencia de la envoltura común, que describe cuán eficientemente se utiliza la energía orbital durante la evolución de la envoltura común para expulsar la envoltura, es pequeña y si los sesgos observacionales afectan la muestra observada.

Concluyo que el dínamo impulsado por la cristalización es probablemente el escenario más plausible para la generación del campo magnético en enanas blancas, pero se requieren simulaciones más detalladas que incluyan transferencia de masa estable para poner a prueba esta hipótesis.

Abstract

For numerous years, the question has persisted regarding why certain white dwarfs possess strong magnetic fields while others do not. Several theories have been formulated to explain the generation of these magnetic fields. The fossil field scenario postulates that magnetic fields observed in white dwarfs originated during the prior stages of Ap or Bp stars. Another proposal involves double degenerate core mergers, where the merging of two white dwarfs results in the creation of robust magnetic fields. An alternative theory suggests that a dynamo is generated during the common envelope phase of a binary system. In this scenario, the differential rotation in the common envelope surrounding the two stars is able to drive a dynamo, thereby giving rise to the white dwarf magnetic field. Over the past decade, a new theory has emerged as a plausible explanation for magnetic fields in white dwarfs. According to this theory, the dynamo is driven by the crystallization of the white dwarf coupled with rapid rotation. As soon as a carbon/oxygen (C/O) white dwarf is crystallizing, the solid core becomes rich in oxygen while the carbon rich outer zones become convective. This situation resembles that of the Earth, in which a solid iron core surrounded by a liquid convection zone together with rotation drives a magnetic dynamo that is supposed to generate the Earth's magnetic field. Based on this analogy it has been proposed that a similar dynamo mechanism is responsible for the development of strong magnetic fields in white dwarfs.

The aim of this thesis is to contrast two theories: one proposing the generation of a dynamo within the common envelope, and the alternative theory suggesting a dynamo driven by the processes of crystallization and rapid rotation. This examination will involve a comparative analysis with observational data.

To accomplish this project, a modified `BSE` code was employed to generate a significant population of close white dwarf binary systems that formed through two common envelope phases. Subsequently, simple scaling equations for the strength of the magnetic field generated through a dynamo within the common envelope and the crystallization dynamo were used to predict the fraction and field strengths of white dwarfs in close double white dwarf binaries. Comparing the prediction of our population model with the observations of double white dwarfs, we obtain the following results. First, two common envelope phases cannot represent the main formation channel for

the currently observed double white dwarf population because the predicted white dwarf masses differ substantially. For a full understanding of the double white dwarf population in general and their magnetic fields in particular, population models that include stable mass transfer are highly required. Second, the common envelope dynamo theory predicts far too many strongly magnetic white dwarfs compared to the observations as well as a relation between orbital period and field strength which is not observed. Even if only a relatively small fraction of double white dwarfs form through two common envelope phases, the common envelope dynamo in its current form can be excluded to properly describe the generation of magnetic fields in double white dwarfs. Third, the predictions of the crystallization driven dynamo could be in agreement with the observations if the common envelope efficiency, which describes how efficiently orbital energy is used during common envelope evolution to expel the envelope, is small and if observational biases affect the observed sample.

I conclude that the crystallization driven dynamo is probably the most plausible scenario for the magnetic field generation in white dwarfs but that more detailed simulations including stable mass transfer are required to further test this hypothesis.

Contents

List of Figures

List of Tables

Chapter 1

Introduction

The vast majority of all stars in our Galaxy will end their lives as white dwarfs. White dwarfs are the Earth-size burned out cores of giant stars in which the pressure balancing gravity is provided by electron degeneracy. Understanding white dwarf stars represents an important part of stellar evolution. One of the fundamental characteristics of white dwarfs is the strength of their magnetic field. Some white dwarfs are strongly magnetic, with field strengths that are a hundred million times stronger than that of the Earth. In contrast, other white dwarfs are non-magnetic, that is, their magnetic fields are so weak that even the most sensitive methods fail to detect them.

The first magnetic field of a white dwarf was discovered more than 50 years ago (Kemp et al., 1970) and thanks to large scale observational surveys such as the Sloan Digital Sky Survey (SDSS) and Gaia, today we know hundreds of strongly magnetic ($B > 1\,\mathrm{MG}$) white dwarfs (Schmidt et al., 2003; Ferrario et al., 2015; Gentile Fusillo et al., 2019; Tremblay et al., 2020). Despite these fantastic observational discoveries, we still do not understand the mechanisms that are responsible for the generation of these strong magnetic fields. It remains therefore completely unclear why some white dwarfs are strongly magnetic while others seem to be essentially non-magnetic.

In this thesis, I aim to contribute to solving this puzzle by taking a detailed look at the occurrence of strongly magnetic white dwarfs in close double white dwarf binary systems and by comparing the properties of the observed sample with current formation theories that include the generation of the magnetic field.

I start by providing a brief review of the most important stages of stellar evolution, as understanding stellar evolution is in addition to mass transfer, the key ingredient for understanding white dwarf binary formation and evolution.

1.1 Star formation

All stars follow different evolutionary paths depending on their mass. Following the initial collapse of a molecular cloud, fragmentation, the second nearly free fall collapse (generated by the dissociation of hydrogen molecules in the core of the protostar), and after the surrounding cloud has been dispersed, protostars appear in the Hertzsprung-Russel diagram on the famous Hayashi track. Stars on the Hayashi track are fully convective (Palla, 2012), For stars with masses exceeding one solar mass, the central temperature of the star increases, and the ionization levels increase, leading to a reduced opacity in this region. Consequently, a radiative core forms which progressively covers a greater portion of the star's mass. At the minimum luminosity, while following the descending path along the Hayashi track, the existence of a radiative core facilitates the escape of energy to the convective envelope, causing the star's luminosity to rise again. Simultaneously, the temperature continues to increase due to the ongoing contraction of the star.

When the luminosity starts to rise again the temperature near the core increases sufficiently to initiate nuclear reactions, although not instantaneously, at a rate required for thermal equilibrium. At the beginning, the CNO chain, converting nearly all the Carbon to Nitrogen, dominates the production of nuclear energy (Salaris and Cassisi, 2005). Given the strong temperature dependence of CNO burning, the core switches again to convective heat transport. As time progresses, nuclear reactions contribute increasingly to the overall luminosity, while the energy production resulting from gravitational collapse becomes less significant in terms of luminosity contribution.

At the local maximum in luminosity in the Hertzsprung-Russell (H-R) diagram (the short dashed line in Figure 1.1), the increasing rate of nuclear energy production causes the core to expand and the energy production to exceed the luminosity (Bernasconi and Maeder, 1996). This causes the gravitational energy to become negative and as a consequence, the star slightly expands while its temperature decreases. The star has reached the main sequence.

For stars with masses lower than the Sun, the evolution is slightly different. For stars with masses, $M \lesssim 0.35\,M_\odot$ the core never becomes radiative. This is because the central temperature never reaches values large enough to burn hydrogen efficiently.

Objects with masses below $0.072\,M_\odot$ but above $0.013\,M_\odot$ are called Brown Dwarfs. These objects burned deuterium during their formation but never reached the stage of stable hydrogen burning (Matthews et al., 1995).

For massive stars, the central temperature becomes rapidly high enough to burn hydrogen into helium, this means that these stars leave the Hayashi track at higher luminosities and evolve almost horizontally along the H-R diagram.

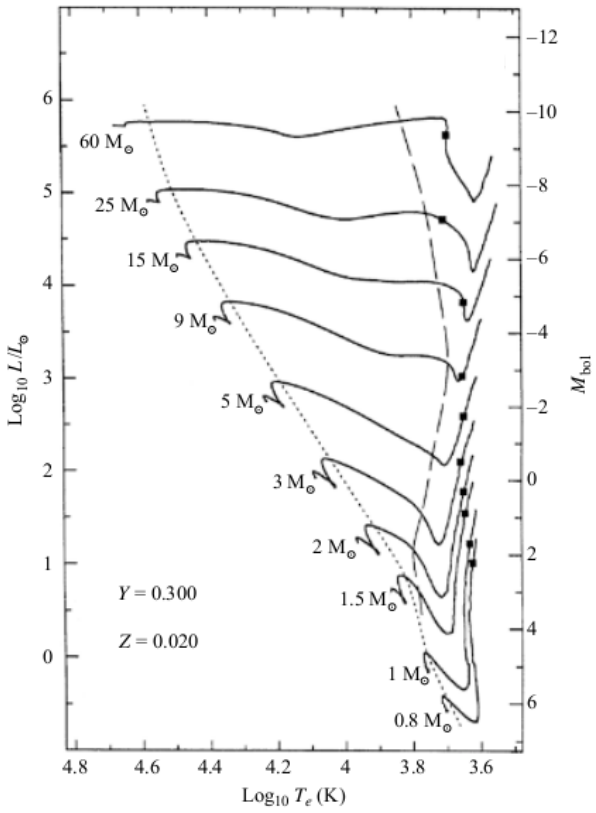

Figure 1.1: These evolutionary tracks are computed for stars with different masses with the composition $X = 0.68$, $Y = 0.30$, and $Z = 0.02$. The tracks usually have the direction from low to high effective temperature (from right to left). The long-dash line represents the point on each track where the convection in the envelope stops and the envelope becomes purely radiative. The short-dash line marks the onset of convection in the core of the star. The squares represent where the onset of deuterium burning in these calculations.

1.2 Main sequence evolution

When stars of different masses reach for the first time the main sequence and start to burn hydrogen in equilibrium, they form the Zero Age Main Sequence (ZAMS). Low mass stars reach the ZAMS on a longer time scale than the more massive ones, i.e., a star with a mass of $60\,M_\odot$ reaches the ZAMS in $28,000$ years, and a star of $0.8\,M_\odot$ reaches the ZAMS at an age of 68 Myrs.

Stars on the ZAMS with masses greater than $1.2\,M_\odot$ exhibit convective cores due to the strong temperature dependence of the CNO cycle. In contrast, hydrogen burning in stars with masses less than $1.2\,M_\odot$ is primarily governed by the PP chain, which is less sensitive to temperature. Consequently, ZAMS stars within the mass range of $0.35\,M_\odot$ to $1.2\,M_\odot$ possess radiative cores and convective envelopes. With decreasing mass, the outer convection zone extends more and more from the surface to the interior, until at a mass of $0.35\,M_\odot$, stars are fully convective (Somers and Pinsonneault, 2015).

For stars like the Sun, it is observed that their luminosity, radius, and temperature steadily increase after they reach the ZAMS. During this evolutionary phase, the helium content in the core increases which implies an increase of the mean molecular weight. As a consequence, the stellar core undergoes compression, leading to an increase in core density. Gravitational potential energy is released, with half of the energy being radiated away and the other half being utilized to raise the thermal energy, and consequently, the gas temperature. This temperature increase has a significant effect on the region of the star where nuclear reactions occur, causing it to expand slightly during the main sequence phase of evolution. Additionally, the rise in temperature and density within the star more than compensates for the decrease in the hydrogen mass fraction, resulting in a gradual increase in the star's luminosity, along with its radius and effective temperature (Iben and Livio, 1993).

1.3 Post main sequence evolution

The final stage of the main sequence phase occurs when the star exhausts its hydrogen fuel in the core. In the case of a $1\,M_{\odot}$ star, as the core contracts due to the ongoing hydrogen shell burning and fuel consumption, the envelope experiences a temperature increase caused by the core's contraction. Consequently, the envelope begins to produce more energy than the core, resulting in an increase in luminosity, a slight expansion of the envelope, and a decrease in effective temperature. Figure 1.2 shows the path that takes the star until reaches the white dwarf phase, also the different processes that experience the star with a mass of $1\,M_{\odot}$.

On the other hand, for a $5\,M_{\odot}$ star, the entire star undergoes a general contraction on the Kelvin-Helmholtz timescale. During this contraction phase, the release of potential gravitational energy leads to a slight increase in luminosity. Eventually, the temperature outside the core rises sufficiently to ignite a thick hydrogen-burning shell. Due to the rapid ignition of the shell, the envelope expands slightly, absorbing some of the released energy from the shell. As a consequence, there is a temporary decrease in luminosity and a corresponding reduction in effective temperature (Schrinner and Deinzer, 2001).

The subsequent evolutionary phase is known as the subgiant branch (SGB). Here, low and intermediate-mass stars ($1 - 3\,M_{\odot}$) still consume the hydrogen that remains at the base of the envelope, while the helium-core steadily increases in mass and becomes almost isothermal, then, when reaching the Schönberg-Chandrasekhar limit, the core starts to rapidly contract and speed up the evolution on the Kevin-Helmholtz timescale. The release of gravitational energy by the core which contracts rapidly makes the envelope of the star expand and the effective temperature decrease. While the core shrinks a strong temperature gradient is established quickly because of the release of the gravitational potential energy. At the same time, the burning hydrogen shell

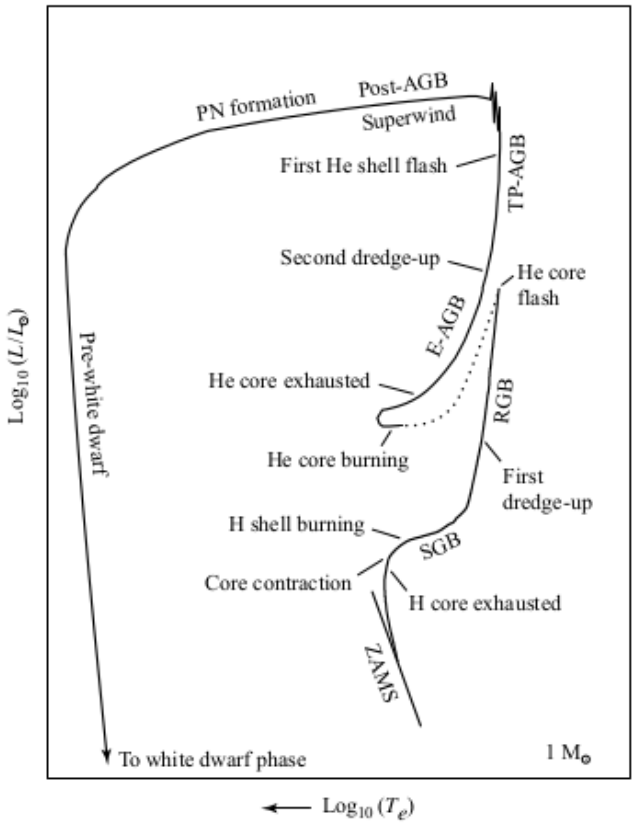

Figure 1.2: Illustration of the evolutionary path of a $1\,M_{\odot}$ star, starting from the ZAMS until it reaches the white dwarf stage. The dotted line represents the stage where a rapid evolution occurs following the helium core flash. Each stage of the star is listed in the diagram.

increases its temperature and density, and even though the shell starts to become thin the rate at which the energy is generated by the shell is increasing fast. The envelope expands again absorbing some of the energy produced by the shell before the energy reaches the surface (Bloecker, 1995).

For more massive stars with $\sim 5\,M_{\odot}$ a thick hydrogen-burning shell is established immediately after the general contraction, the expanding envelope absorbs enough energy for some time to let the luminosity slightly decrease before it recovers.

Figure 1.3 illustrates that following the sub-giant branch, stars enter the red giant phase. In stars with low and intermediate mass, the zone close to the surface develops a convection zone since the effective temperature decreases and the photospheric opacity increases. While the evolution continues, the base of the convection zone spreads deep into the star and transports materials from deep inside to the surface of the star, which is known as the first dredge-up phase (Charbonnel and Palacios, 2003). For stars with lower masses than $1.8\,M_{\odot}$, there is a phase known as helium-core flash, where a huge amount of energy is released for a few seconds, but most of the energy does not even reach the surface but is absorbed by the outer layers of the envelope, causing mass loss from the surface of the star. After the helium flash, the star enters the horizontal

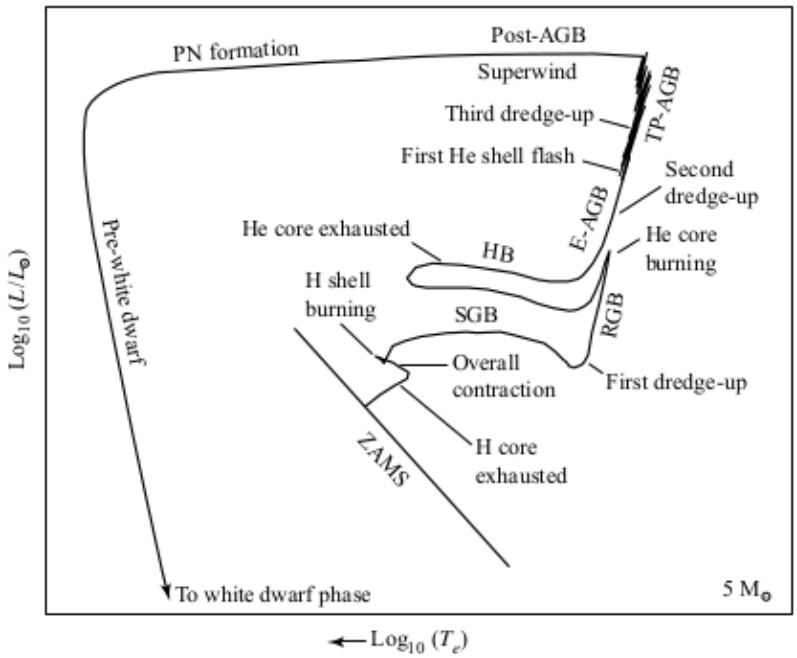

Figure 1.3: Evolutionary path of a star with a mass of $5\,M_{\odot}$. In stars with intermediate mass, the carbon/oxygen (C/O) core becomes degenerate and their late evolution is qualitatively similar to low mass. These stars progress along the asymptotic giant branch. The AGB represents a brief yet crucial phase marked by rich nucleosynthesis and substantial mass loss. Eventually, this mass loss strips away the stellar envelope, leaving behind the degenerate C/O core. This core, following a brief transition as the central star of a planetary nebula, evolves into a long-lived cooling white dwarf.

branch, the envelope shrinks while the energy production decreases. The star's luminosity remains nearly constant but the effective temperature increases. The horizontal branch loop ends when the helium core is exhausted, that is when most of the helium in the core has been converted to carbon and oxygen. The presence of a degenerate carbon/oxygen (C/O) core increases the energy production which first causes the star to cool and expand. The evolutionary tracks enter the path known as the asymptotic giant branch (AGB) which can be thought of as a helium-burning shell analogous to the hydrogen shell-burning red giant branch. It is named asymptotic giant branch because the evolutionary path moves towards the red giant branch asymptotically from the left. This entire evolution path can be observed in Figure 1.2 for stars with $1\,M_{\odot}$ and Figure 1.3 for stars with $5\,M_{\odot}$ (Data from Schaller et al. (1992)). The Thermal-Pulse Asymptotic Giant Branch (TP-AGB) represents the upper segment of the Asymptotic Giant Branch (AGB). In this phase, the helium-burning shell undergoes quasi-periodic cycles of activation and deactivation. This behavior is triggered by helium flashes, wherein the heating of the helium shell causes a surge, pushing the hydrogen shell outward and resulting in a temporary temperature decrease. Subsequently, the helium-burning shell weakens, empowering the hydrogen-burning shell, and the cyclic process

repeats itself.

For stars with $1\,M_\odot$ and $5\,M_\odot$ the evolutionary path turns to the left, almost completely horizontally, in H-R diagram. Following the AGB phase, as the star continues its course on the H-R diagram, the residual gas shell enveloping the central star transforms into what is known as a planetary nebula. The appearance of these nebulae varies, displaying forms that range from simple spheres to more complex structures like rings (Soker, 2002). The diversity in shapes is influenced by factors such as the observer's angle of view and the presence of angular momentum within the system. These planetary nebulae represent a visually captivating and dynamic stage in the stellar life cycle, adding a unique dimension to our understanding of stellar evolution.

The remaining hot central object will become a white dwarf star. Depending on the initial masses of the star, the stellar remnant can be either helium, carbon/oxygen, or oxygen/neon white dwarf. This thesis specifically explores intermediate-mass stars, with masses ranging from 1.0 to $8.0\,M_\odot$. The reason for focusing on these stars is that they will evolve into white dwarfs. Larger initial masses lead to the formation of neutron stars or black holes.

1.4 White Dwarfs

White dwarfs are remnants of stars born with masses lower than $\sim 8\,M_\odot$. White dwarfs are positioned at the bottom left part of the H-R diagram (Figure 1.4) with temperatures from $6,000$K up to $100,000$K, and luminosities from initially a few $L_\odot$ down to a less than a per cent of a solar luminosity. White dwarfs are the burned-out cores of previously hydrogen and helium-burning stars that are unable to start carbon-burning. In white dwarfs, the pressure to balance gravity is provided by electron degeneracy. White dwarfs slowly contract but the released energy is used to increase the Fermi energy (Saumon et al., 2022). For this reason, white dwarfs will eventually cool down and consume their stored thermal energy, fainting slowly away. At temperatures below $\sim 10,000\,$K, C/O white dwarfs crystallize, that is, the atoms in the core start to be ordered in a lattice structure. As we shall see, the crystallization of white dwarf cores might play an important role in the generation of white dwarf magnetic fields.

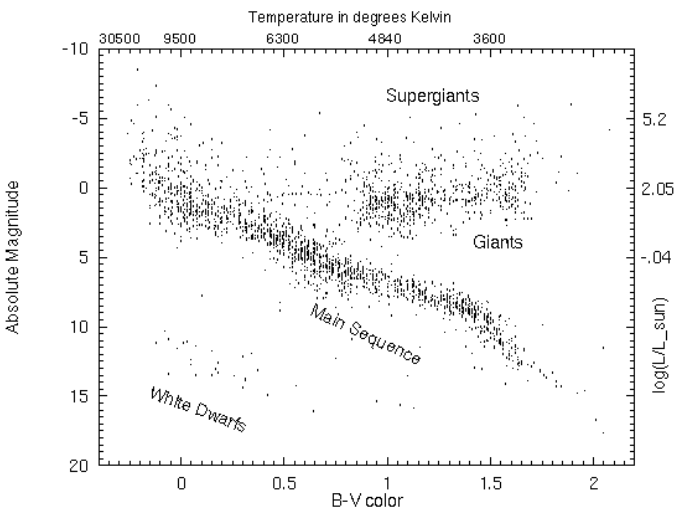

Figure 1.4: The location of white dwarfs in H-R diagram. The faintest detected white dwarfs have a luminosity of approximately $10^{-4.5}\,L_{\odot}$ while younger white dwarfs can have luminosities significantly exceeding that of the sun. White dwarf temperatures range from $6,000$K to $100,000$ K.

White dwarfs are an important tool to understand stellar populations in our Galaxy and they are chronometers of the galaxy that hosts them (van Oirschot et al., 2014). White dwarfs have been studied intensively in recent decades because of their role in several vital research areas of modern astrophysics. For instance, we know that white dwarfs in binary star settings are the progenitors of supernovae Type Ia while the exact evolutionary channel that leads to these important explosions is still unknown. In the single-degenerate model, the mass is transferred from a non-degenerated star onto a white dwarf, while in the double-degenerate model, two white dwarfs merge (Wheeler, 2012). White dwarfs in binaries are also predicted to form the dominant population of gravitational wave sources to be detected with space interferometers such as LISA (Lamberts et al., 2019). During the last years, white dwarfs have also become important objects for planetary science, as the metal lines frequently observed in the spectra of white dwarfs are thought to be generated by the accretion of planetary debris. White dwarfs are the central objects for this thesis and it is therefore appropriate to briefly describe the observational appearance of white dwarfs.

During their lives, white dwarfs emit mostly in the wavelength range from extreme ultraviolet to near-infrared wavelengths and are usually classified by the features in their spectrum, which differs from those observed in main sequence stars. White dwarf atmospheres are mostly formed of hydrogen and helium and the observed absorption lines are very broad because of pressure broadening (van Horn, 1984). Different classifications of white dwarfs based on the spectrum are listed in Table 1.1 and the D in almost all of these spectral types indicates the degeneration of electrons.

1.5 Formation of close white dwarfs binaries

In a binary system, two stars orbit around the system's center of mass. The Roche approximation is applied, assuming a circular orbit for the binary and treating the gravitational fields of both stars as point masses. The volumes enclosed by the critical surfaces for each star are referred

DA	These white dwarfs only show hydrogen lines. The letter A indicates the existence of strong Balmer lines. If weak metal lines are also detected, the white dwarf is called DAZ. DA temperatures range from $6,000\,\mathrm{K}$ to more than $100,000\,\mathrm{K}$
DB	DB white dwarfs only show helium lines. The letter B indicates that strong neutral helium lines are detected. If weak Ca II lines or other metal lines are observed, the white dwarf is called DBZ. DB white dwarf temperature ranges from $10,000$ to $30,000\,\mathrm{K}$.
DC	These white dwarfs show featureless spectra. Their effective temperatures are below $10,000\,\mathrm{K}$ where the helium lines become invisible at optical wavelength. At even lower temperatures also the Balmer lines disappear.
DO	The temperature of these white dwarfs ranges from $45,000$ to $100,000\,\mathrm{K}$. The spectra are dominated by helium lines but some of them also show hydrogen lines.
PG1159	These are the hotter white dwarfs, between $75,000$ to $200,000\mathrm{K}$. They have hydrogen-deficient atmospheres and are characterized by absorption lines of He II, carbon, and highly ionized oxygen.
DZ	These white dwarfs show helium lines and lines from heavy elements mostly calcium, followed by magnesium and iron. These latter elements should not stay at the outer layers over time because of the gravitational settlement time scale, which is short compared with the cooling time scale. The observed elements therefore cannot be primordial but must be supplied by the exterior. DZ can be considered as the helium-rich equivalent to DAZ white dwarfs.
DQ	These white dwarfs show carbon lines. There are three types of these white dwarfs, hot ($18,000 < T_{eff} < 24,000\,\mathrm{K}$), warm ($10,000 < T_{eff} < 18,000\,\mathrm{K}$), and cold ($T_{eff} < 8,000\,\mathrm{K}$) DQ. Interestingly, the warm and hot DQ white dwarfs show the presence of strong magnetic fields.

Table 1.1: White dwarf classification by spectral features.

to as Roche lobes. In most main sequence binary stars the orbital separations are so large that neither of the two stars fills its Roche lobe during stellar evolution, not even on the AGB. These wide binary stars typically form wide double white dwarfs when the two stars evolved off the main sequence (Nelemans et al., 2001). In such cases, the evolution of the stars is not affected by the presence of the companion.

However, the situation changes when the separation of the initial main sequence binary is small enough for the two stars to interact which is supposed to happen in about one quarter of all main sequence binary stars. When one of the stars fills its Roche lobe, mass transfer to its companion begins through the inner Lagrangian point L_1, where the two Roche lobes make contact (Iben and Livio, 1993). In general, understanding the consequences of mass transfer on the evolution of

binary stars represents a fundamental part of stellar evolution. For this thesis, mass transfer is of fundamental importance because the topic of my work is close double white dwarfs which evolve through two phases of mass transfer. Mass transfer can be unstable on different time scales and it can be driven by these instabilities of additional processes such as the nuclear evolution of one of the stars or orbital angular momentum loss of the binary star (Soberman et al., 1997). Mass transfer can be conservative which means that all the mass and angular momentum is kept in the binary stars system or non-conservative which means that mass and angular momentum are lost as a consequence of the mass transfer process. In what follows I briefly describe the main modes of mass transfer.

1.5.1 Mass transfer in binary stars

Different types of mass transfer have been extensively studied and analyzed in the review article by Belloni and Schreiber (2023), which provides valuable insights into the underlying mechanisms and principles governing mass transfer. Through a comprehensive exploration of these categories of mass transfer, we aim to broaden our understanding of mass transfer in general and its practical applications in binary studies in particular.

Dynamical time-scale mass transfer

Categorization of mass transfer can be achieved by comparing the two logarithmic derivatives associated with the donor star radius and the Roche lobe radius. The difference between the adiabatic and Roche lobe radius-mass exponent can distinguish between dynamically stable and unstable mass transfer. If the difference is positive, the mass transfer is dynamically stable, indicating that as a consequence of the mass transfer, the radius of the donor star in hydrostatic equilibrium is smaller than the Roche lobe radius. Conversely, if the difference is negative, the mass transfer is dynamically unstable. In the case of dynamically unstable mass transfer, two main outcomes may arise. If the donor is a main-sequence star or a degenerate object, the binary will most likely merge at the donor's dynamical time scale, with a non-negligible fraction of the total mass being lost in such an energetic event. However, if the donor has evolved beyond the main sequence, it will trigger common envelope evolution, leading to a substantial decay in the orbital period. The outcome of common envelope evolution can be a merger as well or, if sufficient orbital energy is available to expel the envelope before the two stars merge, a post common envelope binary consisting of compact objects with a main sequence star companion (Ge et al., 2010, 2015; Belloni and Schreiber, 2023).

Thermal time-scale mass transfer

The perturbation of thermal equilibrium occurs in response to mass loss and can be restored only if the mass transfer occurs slowly enough for the donor's interior to relax to thermal equilibrium. Otherwise, the mass transfer will be thermally unstable, taking place on the thermal time scale of the donor. In such cases, the radius-mass exponent of the thermal equilibrium is compared to the Roche lobe radius exponent, and knowledge of the mass-radius relation of stars in thermal equilibrium is required. If the thermal equilibrium radius-mass exponent is greater than the adiabatic and the Roche lobe radius-mass exponent, the mass transfer must be driven by an external process and will take place on a time scale different from the dynamical and thermal time scales. On the contrary, if the equilibrium radius-mass exponent is lower than the adiabatic and larger than the Roche lobe radius-mass exponent, the mass transfer will be driven by the thermal readjustment and will take place at the donor's thermal time scale (Schenker and King, 2002; Wijnen et al., 2015; Belloni and Schreiber, 2023).

Nuclear or orbital angular momentum loss time-scale transfer

The transfer of mass between stars can be brought about by the nuclear expansion of the donor star filling its Roche lobe or by the loss of orbital angular momentum causing the Roche lobe of the donor to shrink in response to the mass loss. If the mass transfer is due to nuclear expansion, it occurs at a velocity such that the donor radius is similar to its Roche lobe radius. If the mass transfer is caused by the loss of orbital angular momentum, the rate of mass transfer depends entirely on the strength of the orbital angular momentum loss. The two primary mechanisms of angular momentum loss that drive binary evolution are gravitational wave radiation and braking by magnetic winds, although the latter is not fully understood. Additionally, there are other ways in which angular momentum loss occurs in interacting binaries that arise as a consequence of the mass transfer, known as consequential angular momentum loss. Frictional angular momentum loss occurs due to fast isotropic winds and isotropic re-emission from the interaction of expelled material and the accretor/donor. The latter represents a form of consequential angular momentum loss (Sen et al., 2022; Belloni and Schreiber, 2023).

1.5.2 Common envelope evolution

When mass transfer in a binary system is dynamically unstable, the accreting star is unable to assimilate all the matter transferred from the donor star. Instead, this excess matter accumulates, causing the accretor's Roche lobe to be exceeded, leading to the development of a common envelope. In this common envelope, both the core of the donor star and the companion exist, surrounded by a

shared envelope. This situation typically arises when the donor star is a giant or a supergiant with a convective envelope. Stars with convective envelopes tend to expand or at least not shrink when losing mass, while the Roche lobe radius contracts as mass is transferred from the more massive to the less massive star. This causes the donor star to fill its Roche lobe progressively, leading to uncontrolled mass transfer on a dynamical timescale, known as dynamical mass transfer. Once a common envelope system forms, the friction between the binary components and the envelope causes them to spiral toward each other until sufficient orbital energy is released, ultimately ejecting the envelope. This concludes the spiral-in phase, resulting in a binary system with a shorter orbital period, typically between $0.1 \sim 10$ [days], consisting of the core of a giant and a normal secondary star. In general, common envelope evolution tends to produce systems with very short orbital periods (Paczynski, 1976).

Common envelope evolution is an important phase of stellar evolution but is not fully understood. Consequently, to estimate the outcome of common envelope evolution, simple energy conservation equations are used. Among these equations, Equation 1.1 stands out as the most widely employed, which works for simulating detached post common envelope binaries (PCEBs) and for the reconstruction of the evolutionary history of the observed PCEBs population. In this approximation, the binding energy (E_{bind}), which is the necessary energy to unbind the envelope, is compared with the change in orbital energy because of the common envelope phase (ΔE_{orb}) scaled with an efficiency α_{CE} which takes into account possible energy losses (e.g. due to radiation). The key equation for common envelope evolution is thus:

$$E_{bind} = \alpha_{CE} \Delta E_{orb} \tag{1.1}$$

Han et al. (1995a) suggests that the values of the efficiency parameter are $\alpha_{CE} \sim 0.3$ or 1.0, although Livio and Soker (1988) say that 0.3 is more appropriate but still quite conservative. If we consider a value of α_{CE} as high as 1.0, for example, this means that the process is efficient, which means that all the energy that can be extracted from the orbit of the binary is used to expand the common envelope and eventually eject it. On the other hand, if the α_{CE} has a value of 0.3 this means that only the 30% of the available orbital energy was used for this ejection, and the other 70% was lost in other processes.

The most basic expression for the values of the binding energy involved in the evolution of the common envelope comes from the potential gravitational energy of the envelope:

$$E_{bind} = -\frac{G M_1 M_{1,e}}{\lambda R_1} \tag{1.2}$$

where M_1, $M_{1,e}$, R_1 are the progenitor white dwarf mass, the envelope mass, and the radius at the onset common envelope phase while λ is the structural parameter that depends on the specifics

of the mass distribution of the star and its radius, which was often assumed to be constant but this represents an oversimplification of the problem. Loosely bound envelopes like the ones that we can find in more evolved stars (e.g. close to the tip of the AGB), can reach higher values of λ, while more compact envelopes are better approximated by a smaller λ value. Changes in the binding energy can also occur if more energy sources are involved in the ejection of the envelope, the most important one being most likely recombination energy (Zorotovic et al., 2014b).

While Equation 1.2 is a useful approximation if we want to include information from the internal structure of the star and other forms of energy that may contribute we may need a different approach. If a fraction α_{rec} of the recombination energy of the envelope contributes to the ejection process, the binding energy can be rewritten as follows:

$$E_{bind} = -\int_{M_{1,c}}^{M1} \frac{Gm}{r(m)} dm + \alpha_{rec} \int_{M_{1,c}}^{M_1} U_{rec}(m) dm \tag{1.3}$$

where $M_{1,c}$ is the core mass of the primary and $r(m)$ the radius that enclosed the mass m.

On the other hand, Han et al. (1995a) introduces the parameter α_{th} due to the uncertainty of what fraction of thermal energy is used in the ejection of the common envelope, so a more general envelope binding energy can be expressed as:

$$E_{bind} = -\int_{M_{1,c}}^{M1} \frac{Gm}{r(m)} dm + \alpha_{th} \int_{M_{1,c}}^{M_1} U_{th}(m) dm + \alpha_{rec} \int_{M_{1,c}}^{M_1} U_{rec}(m) dm \tag{1.4}$$

The values of α_{th} and α_{rec} are essential for determining the binding energy. Large values of these efficiencies lead to loosely bound envelopes while small values imply larger binding energies (Dewi and Tauris, 2000).

Observations of post common envelope binaries show that in most cases orbital energy is sufficient to reproduce the formation of the binary. Only in a few cases, it is needed, in order to explain the existence of the binary, to increase the energy available during the common envelope phase. Davis et al. (2010) presented an example where the binary orbital energy is not enough to justify the survival of the IK Peg system until reaches the PCEB stage. They compute that the efficiency α_{CE} required to justify the observation must be in the range of $\alpha_{CE} \gtrsim 3$, which is nonphysical. A possible explanation consists of considering additional energy sources, like the total internal gas energy and ionic recombination processes. The parameter that was used to represent the efficiency with which the recombination energy contributes to the process of ejection of the common envelope is indicated as α_{rec}. A value of α_{rec} close to 0 means that the ejection of the common envelope is mostly fueled by the orbital energy of the binary. In consequence, a larger number of binaries will end their life merging, so they cannot be counted as binary systems. In the other case, if α_{rec} is close to 1, this corresponds to a larger efficiency of using recombination

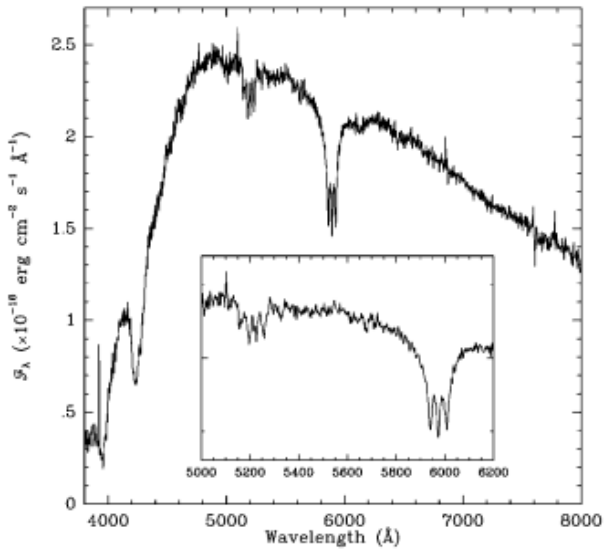

Figure 1.5: This figure is the spectrum taken in the Keck II telescope using the Low-Resolution Imaging Spectrograph (LRIS) which shows strong Ca II, Ca I, Mg I, and Na I lines. The Zeeman splitting is examined in the inset. Credit to Reid et al. (2001).

energy which occurs in clouds that are opaque for the emitted radiation (Davis et al., 2010). If recombination energy contributes, less orbital energy is needed, which results in a larger fraction of binaries surviving common envelopes evolution. This situation can be observed in Figure 5.1, in the center and the left-hand plots, where the α_{CE} is fixed and the α_{rec} is changed. In this work, we used α_{CE} as α and its values are 0.3 and 1.0, and α_{rec} with values of 0.0 and 1.0.

1.6 Detecting magnetic fields in White Dwarfs

The first detection of a magnetic field in a star beside the Sun occurred in 1947 and was obtained by Horace Babcock. He detected the magnetic field of a main sequence A-type star. He and other astronomers established in the early 1969s that magnetic fields appear at the surface of a specific class of stars on the upper main sequence (A and B-late type star). After some time, and thanks to the collaboration of several people, in 1969 John D. Landstreet suggested Kemp to study a strange white dwarf called $Gwr + 70^\circ\,8247$ and to investigate if it might be magnetic. Indeed, Kemp et al. (1970) presented a strong signal of circular polarization in two independent observations and it became clear that $Gwr + 70^\circ\,8247$ was the first magnetic white dwarf ever discovered (see Landstreet, 2020, for more details on the history of the discovery).

Polarization of the continuum has been the first method for detecting magnetic fields in white dwarfs. This technique, however, requires relatively strong fields, of the order of at least one

MG. For white dwarfs with helium-rich atmospheres that exhibit He I spectral lines, magnetic field intensities can be determined by analyzing the atomic helium lines, which is a more challenging technique. For some white dwarfs with carbon-rich atmospheres and field strengths in the range of 100 MG, polarimetry has been used to make the measurements. Circular spectropolarimetry can be also used as an alternative method for measuring magnetic fields in cases where the Zeeman split is weak and unresolvable. By analyzing the change in the sign of the circular polarization along spectral lines, it is possible to detect fields of the order of kilo-Gauss (Ferrario et al., 2020). This method has been used to explore the fraction of magnetic white dwarfs in a volume limited sample (Bagnulo and Landstreet, 2020).

The presence of a magnetic field can also be established by the detection of absorption lines affected by the Zeeman effect (split). The lines that are split can come from atmospheric hydrogen, carbon, or other metals. An example is shown in Figure 1.5. As previously mentioned, the majority of magnetic white dwarfs are rich in hydrogen, and detection of their magnetic fields often involves spectroscopic measurements using Zeeman splitting for the Balmer hydrogen series. In fact, at low magnetic field intensities, the splitting of these lines exhibits linear dependence on the field intensity. However, as the field intensity increases, the contribution of nonlinear terms becomes increasingly significant, making a determination of the field intensity more complex. In particular, the quadratic terms play a crucial role for field intensities on the order of ~ 1 MG, and for higher field intensities, the situation becomes even more complicated due to the tangling of subcomponents of the spectroscopic lines in wavelength.

An additional method for measuring magnetic fields in white dwarfs is to analyze the cyclotron emission. The presence of free electrons in the white dwarf's magnetic atmosphere is expected to generate cyclotron thermal radiation, which produces a distinctive absorption feature at the fundamental cyclotron frequency ω_c. The fundamental cyclotron frequency is more likely to be detected in optical to near-infrared spectra of magnetic white dwarfs with fields of 10^7 G or higher. Another approach for detecting cyclotrons is due to polarimetry. The cyclotron emission exhibits 100% circular polarization when viewed along the field lines and is elliptically polarized at other viewing angles.

1.7 Scenarios for the generation of magnetic fields in white dwarfs

The most popular scenarios for the generation of magnetic fields in white dwarfs are the fossil field scenario (Sec.1.7.1), a dynamo generated during a common envelope evolution in close binaries (Sec.1.7.2), coalescing double degenerate cores/objects (Sec.1.7.3), and a new scenario based on a

dynamo mechanism related to the phase separation in carbon-oxygen white dwarfs at the onset of crystallization (Sec.1.7.4).

1.7.1 Fossil Field Scenario

The fossil scenario suggests that high-field magnetic white dwarfs result from the evolution of peculiar stars, Ap and Bp. These kinds of stars possess strong magnetic fields for main sequence stars, around $10^3 - 10^5$ G. Assuming magnetic flux conversation, the field amplification will be around $\simeq 10^4$ when the Ap or Bp stars evolve into a white dwarf which could explain the field strength of magnetic white dwarfs (Angel et al., 1981).

However, the scenario has several serious flaws. In order to establish the viability of the theory, a comparison was made between the space density of magnetic white dwarf stars and the expected space density of the white dwarfs descending from Ap/Bp magnetic stars. The findings of this study indicate that the predicted density of the magnetic nuclei remnants falls within the range of $4 - 8 \times 10^4 pc^{-3}$ which is not enough to explain the relative number of magnetic white dwarfs (Kawka and Vennes, 2004; Wickramasinghe and Ferrario, 2005). In addition, according to the fossil field scenario, it is expected that magnetic white dwarfs would be equally prevalent among both young (hot) and older (cool) white dwarfs while observations suggest that this is not the case. Finally, one of the major challenges of this theory comes from the potential loss of magnetic flux during the post-main sequence evolution. This is due to the fact that the magnetic field emanates from the envelope, and a proportion of this field may be shed during the mass loss phase, leaving behind only a fraction of the magnetic flux from the Ap star.

1.7.2 Dynamo during common envelope

An alternative hypothesis for the formation of magnetic fields is a dynamo triggered during the common envelope phase. This phase, which occurs during the evolution of a binary star, involves a white dwarf nucleus that was once a giant star and an unevolved main sequence star, both enclosed within a shared envelope. It has been theorized that this phase may give rise to progenitors of Supernovae Ia, X-ray binaries, and double neutron stars. The significance of common envelope evolution lies in its potential to enable the formation of a large variety of close binary stars containing compact objects.

There exist several theories regarding the generation of magnetic fields during common envelope evolution. In one idea it has been proposed that differential rotation is responsible for magnetic field generation. This theory suggests that, within the common envelope, the white dwarf and main sequence star have not yet evolved and recently spiraled in towards one another until they were close enough for magnetic braking to induce a semi-detached state, forming a cataclysmic

variable. As these two stars rotate increasingly faster within the slowly rotating common envelope, the differential rotation within the envelope increases. Through the $\alpha - \Omega$ dynamo process, this differential rotation in the envelope may generate strong magnetic fields (Regős and Tout, 1995). The main problem of this idea is that it remains unclear how the field generated in the envelope, which will be expelled, can be captured by the white dwarfs.

The second theory suggests that magnetic fields are generated through an accretion disk. An accretion disk around the white dwarf may form during common envelope evolution and represents an alternative location for the magnetic field generation. Such a disk can form when the companion is perturbed by tidal effects within the common envelope (Nordhaus et al., 2011). In this case, the field reaches the white dwarf as a fraction of the disk material might be accreted by the white dwarf.

Briggs et al. (2018) proposed a simple relation between the generated field strength of the emerging white dwarf and the orbital period of the formed post common envelope binary star. Briggs et al. (2018) claim that this relation can explain the mass and field strength distribution of single magnetic white dwarfs and white dwarfs in binaries. However, Belloni and Schreiber (2020) discovered dramatic discrepancies between the proposed theory and observations, as the magnetic field equation used by Briggs et al. (2018) predicts far too many magnetic white dwarfs in detached white dwarf plus M-dwarf post common envelope binaries and cataclysmic variables.

1.7.3 Double degenerate core mergers

Double degenerate core mergers represent another scenario for the formation of magnetic white dwarfs (García-Berro et al., 2012). It is believed that these merger events could be responsible for creating magnetars and white dwarfs with very strong magnetic fields. According to this scenario, the fusion of two degenerate cores produces a hot, convective, and differentially rotating corona, leading to the production of strong magnetic fields that are confined to the outer layers of the resulting remnant. These magnetic fields do not decay for long timescales. Additionally, this study predicts that white dwarfs with high magnetic fields are massive which is consistent with observation. However, this and the previous scenarios fail to explain the absence of young detached magnetic white dwarfs in close binaries (Liebert et al., 2005) as well as the paucity of strongly magnetic young single white dwarfs.

1.7.4 Rotation and Crystallization Driven Dynamo

According to a rather recently suggested scenario, magnetic field generation in white dwarfs could be driven by rotation and crystallization, which might lead to a magnetic dynamo similar to those suggested to produce the magnetic fields in low-mass stars and planets. Important features of such

dynamos include rotation, density stratification, and an extended convection zone. In the case of white dwarfs, at certain temperatures and densities within the white dwarf, the ions begin to freeze into a lattice structure, causing crystallization. Specifically, the interior of a white dwarf contains plasma ions and degenerate electron gas, and as the carbon and oxygen ions cool below a critical temperature, the core of the white dwarf begins to crystallize. The phase diagram of this mixture initially takes the form of a spindle, which then evolves into an azeotrope before finally reaching a eutectic form. Due to the spindle shape of the C-O mixture phase diagram, the resulting solid after crystallization is richer in oxygen and denser than the liquid (Isern et al., 1997). Therefore, a solid core grows from the inside of the star while the lighter liquid that remains can be redistributed by the Rayleigh-Taylor instabilities. These factors, combined with the rapid rotation of the star, might cause the generation of a strong magnetic field.

Scaling laws can be utilized to infer the magnetic field strength of celestial bodies such as Earth, Jupiter, and low-mass stars. When it comes to magnetic fields generated by dynamos in these bodies, the most promising approach to replicate observed field strengths is considered to be the energy flux scaling law introduced by Christensen et al. (2009). This law is an expansion of a scaling law derived from geodynamo models that applies to rapidly rotating stars exhibiting strong density stratification. It proposes that the magnetic field strength is determined by the flux of energy that is accessible to create the magnetic field. It is not clear if the energy flux scaling law is suitable for white dwarfs as well. In the very fast rotation regime, superequipartition might instead be expected (Ginzburg et al., 2022).

1.7.5 The rotation and crystallization driven dynamo and the evolution of close white dwarf binaries

As shown by Schreiber et al. (2021a), a fraction of strongly magnetic white dwarfs in populations with close binary white dwarfs can not be reproduced by any suggested scenario but the crystallization and a fast rotation driven dynamo. Most of these close binary stars include one white dwarf that formed through a common envelope evolution. The detached binary stars that emerge from the common envelope evolve towards shorter orbital periods driven by the angular momentum loss and eventually, they become semi-detached cataclysmic variable stars. In cataclysmic variables, the companion star fills its Roche lobe which generates mass transfer driven by angular momentum loss.

Polars are cataclysmic variables that contain a strongly magnetic white dwarf and are characterized by the synchronization of the white dwarf's rotation with the orbital motion of the secondary star, due to the interaction of their magnetic fields. A smaller fraction of systems, known as intermediate polar, feature a disruption of the internal regions of the accretion disk caused by the magnetic field

of the white dwarf, without the connection of the magnetic fields of both stars, resulting in a lack of synchronization between the white dwarf's rotation and the orbital motion. Among detached young binary white dwarfs, no instances have been found of a white dwarf with a strong magnetic field. According to some theories, magnetic fields in white dwarfs may be generated during their formation process. As a result, post common envelope binaries that contain a hot white dwarf are expected to exhibit strong magnetic fields. However, this is not observed in reality. If the white dwarf magnetic fields are generated when the white dwarf has sufficiently cooled to crystallize, the observed absence of magnetic fields among young post common envelope binaries, however, can be easily explained.

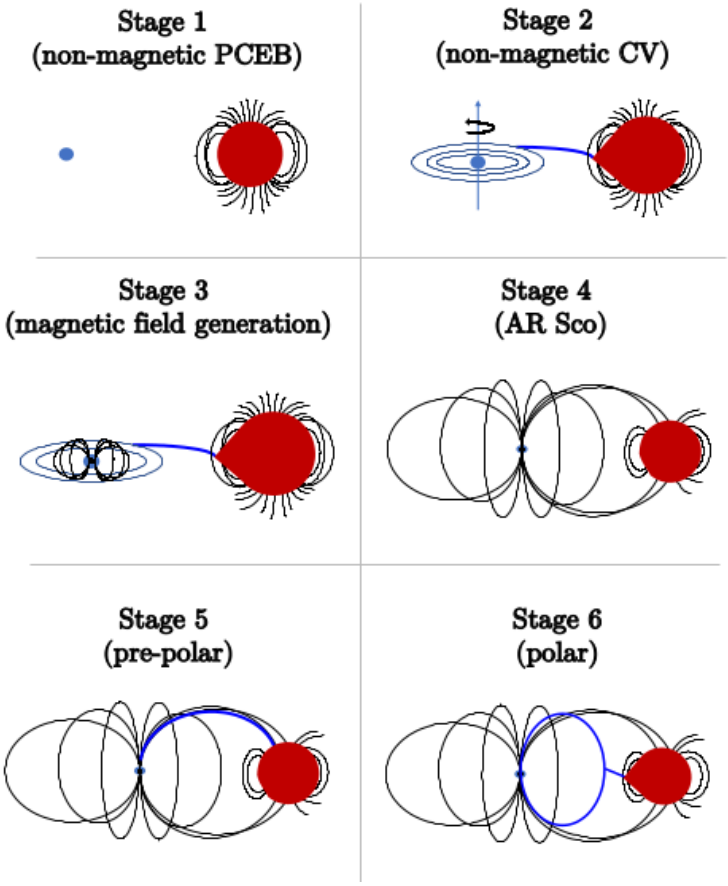

Figure 1.6: The progression of a binary system through evolutionary phases leading to the formation of a polar configuration is illustrated in this diagram (from Schreiber et al. (2021a)). The Figure also highlights the generation of a magnetic field during the crystallization of the white dwarf, where a robust magnetic field is produced through a dynamo process.

Figure 1.6 shows different states of a binary system. In the proposed model, the white dwarf is presumed to originate without a robust magnetic field, aligning with the lack of potent magnetic fields in post common envelope close detached binaries. This constitutes the first phase of the

model. The binary system that lacks magnetic properties advances gradually through orbital periods, with the white dwarfs gradually becoming cooler and potentially crystallizing. Upon the secondary star's Roche lobe filling, the binary system transforms into a cataclysmic variable. The accretion process causes the white dwarf to spin up and both conditions for the dynamo to operate are fulfilled. This sequence of events constitutes the second phase of the model.

In the hypothetical scenario where the before-mentioned conditions are met, the dynamo, which is driven by rotation and crystallization, generates a robust magnetic field, marking the third phase of the model. If the magnetic field is potent enough to establish a connection with the secondary star's magnetic field, this causes a synchronization torque on the white dwarf's spin. As a result, the transfer of spin angular momentum to the orbital motion occurs. In other words, the synchronization torque causes the separation between both stars to increase, and the secondary to detach from its Roche lobe. The link between the magnetospheres of both stars also reduces the loss of angular momentum loss due to the magnetic wind drag. The gas that escapes from the secondary star is accreted by the white dwarf along the connected field lines instead of being expelled from the system.

The onset of synchronization marks the beginning of the fourth phase of the model, leading to the formation of a white dwarf radio-pulsing binary, such as AR Sco (Marsh et al., 2016). In this configuration, the fast-rotating white dwarf's spin rate reduces significantly in a relatively short period of time, estimated to be between $1 - 10\,\mathrm{Myr}$. When the white dwarf's spin becomes synchronized with the secondary star's orbital motion, the binary system evolves into a pre-polar state. In this state, the accretion wind generates cyclotron emission observed as the third harmonic of a fundamental cyclotron emitted by a low-density plasma. This characteristic emission serves as a marker for identifying some magnetic binary white dwarfs, marking the fifth phase of the model. Reduced magnetic braking and the gravitational radiation-induced loss of angular momentum result in the stars moving closer to each other, until the secondary star refills its Roche lobe, culminating in the formation of a polar configuration, marking the sixth and final stage of the proposed model.

The proposed evolution sequence is in agreement with the observations of close binaries that harbor potent magnetic white dwarfs with main sequence star companions. Furthermore, as the conditions that enable the generation of a dynamo are relatively prevalent in cataclysmic variables, the model can effectively account for a significant proportion of cataclysmic variables that feature magnetic white dwarfs. While some detached binaries contain magnetic white dwarfs, the model predicts that these systems were once cataclysmic variables in the past but ceased the mass transfer process due to the emergence of the magnetic field and the transfer of spin angular momentum to

the orbit. The model also explains the absence of strongly magnetic white dwarfs in young post common envelope binaries.

1.8 Census of observations of magnetic fields in white dwarfs

The origin of magnetic fields in white dwarfs is still a topic that is debated or maybe even disputed. The discrepancy in the frequency of magnetic white dwarfs is considerable, with noticeable differences between single white dwarfs and those in binary systems. Additionally, there is also a considerable discrepancy in the strengths of the magnetic fields observed in both categories of white dwarfs.

1.8.1 Single White Dwarfs

Initial studies about possible magnetic fields in white dwarfs were first performed by Blackett (1947), and observational confirmation was provided by Kemp et al. (1970). Magnitude limited surveys, for example, based on the Sloan Digital Sky Survey (SDSS) established that around $2-10\%$ of single white dwarfs show magnetic fields higher than 1 MG.

More recently, Bagnulo and Landstreet (2021a) analyzed a sample of 149 observed white dwarfs finding no correlation between field presence and spectral class, except possibly for DQ and DZ white dwarfs. According to their analysis, the frequency of magnetism appears to increase until cooling times of around 5 Gyr, after which it drops. Bagnulo and Landstreet (2021a) also found that the field strength is uniformly distributed from 40 kG to 300 MG, limiting the range of field strengths frequently found in white dwarfs. Additionally, they discovered that magnetic white dwarfs are more massive than non-magnetic white dwarfs, with marginal evidence that younger magnetic dwarfs are more massive than older ones. Magnetic single white dwarfs can be categorized into two groups based on their magnetic fields: strong magnetic fields with a range of 10^5-10^9 G, which constitute approximately $13\pm4\,\%$ of all white dwarfs, and low magnetic fields below 10^5 G, which occur less frequently.

There are approximately 600 known white dwarfs that possess magnetic fields ranging from 10^3 G to 10^9 G. Among these, the population of white dwarfs with strong magnetic fields has an average mass of $0.784\pm0.047\,M_\odot$, whereas non-magnetic white dwarfs have average masses of $0.6\,M_\odot$.

1.8.2 Magnetic White Dwarfs in Binary Systems

In addition to individual magnetic white dwarfs, there are binary systems where at least one of them is a white dwarf. White dwarf binary stars occur in nature in several different configurations

and the fraction of magnetic white dwarfs differs dramatically in the several sub-classes. Below we provide a brief summary of the currently available observational constraints.

Wide white dwarf plus main sequence

In these systems, both stellar components are too widely separated to have currently or in the past experienced interactions in terms of mass transfer. There are currently only five known systems composed of a magnetic white dwarf plus a main sequence companion in a wide binary star. Only two of these systems are within the 20 pc volume around the Sun. Because this volume contains roughly 30 magnetic white dwarfs, it seems that just a small percentage of white dwarfs in wide binary stars are magnetic. However, the currently known sample is probably highly incomplete because single white dwarfs are more frequently magnetic the cooler they are and cooler white dwarfs are more difficult to identify against a bright main sequence star companion (Landstreet and Bagnulo, 2020).

White dwarf plus M dwarf (PCEBs)

Post common envelope binaries (PCEBs) are close detached binaries where both stars evolved through a common envelope phase. The observed population is dominated by systems with negligible magnetic fields and only well below 10% of these systems contain a strongly magnetic white dwarf. These few magnetic white dwarfs in PCEBs are relatively cool ($\sim$ 10000 K) and very close to filling their Roche lobe. As mentioned previously, this could be related to the fact that these objects have been cataclysmic variables in the past. Alternatively, as the fields have been discovered through cyclotron emission generated by wind accretion, it might be caused by an observational bias. As can be seen in Figure 1.7, all the systems show broad emission features similar to cyclotron lines (Parsons et al., 2021a; Belloni and Schreiber, 2023).

The stellar and binary parameters for these stars are often uncertain, primarily because their spectra are frequently affected by strong cyclotron emission, posing challenges in making direct measurements. Precision in determining fundamental parameters, such as the masses of white dwarfs and Roche lobe filling factors, would offer valuable insights. These measurements could play a crucial role in discerning between pre-cataclysmic variable and temporarily detached cataclysmic variable scenarios (Parsons et al., 2021a).

White dwarf plus M dwarf in a semi-detached configuration

Cataclysmic variables are a compact interacting binary system, where the white dwarf is accreting from a Roche lobe filling the main sequence (or slightly evolved) companion star. The companion is usually a low-mass late-type star. In most cataclysmic variables an accretion disk forms because of the conservation of angular momentum of the overflowing material.

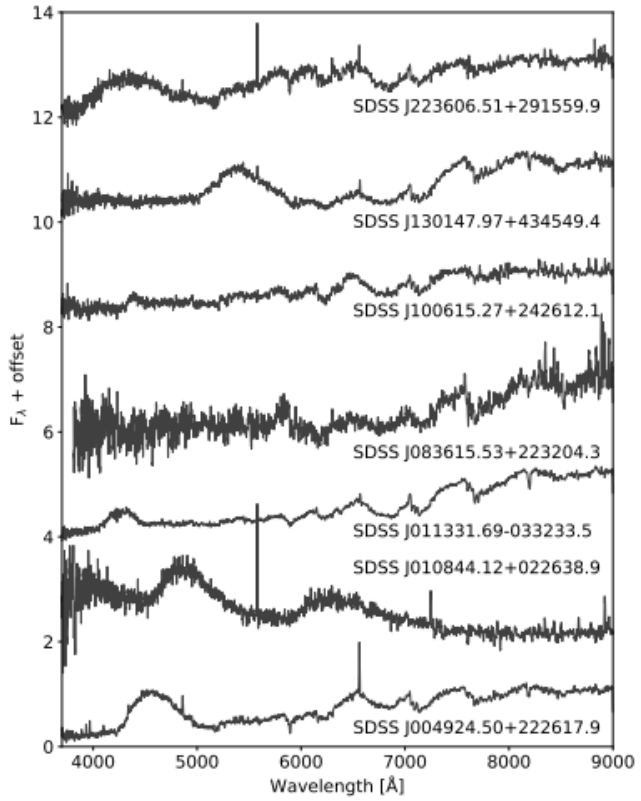

Name	Cyclotron harmonics detected (Å)	Photometric variability
SDSS J004924.50+222617.9	6840, 4560 (n = 2, 3)	355 mins
SDSS J010844.12+022638.9	6450, 4850 (n = 3, 4)	81 mins
SDSS J011331.69-033233.5	6380, 4250 (n = 2, 3)	263 mins
SDSS J083615.53+223204.3	5830 (n = 1 or n = 2)	No data
SDSS J100615.27+242612.1	6530, 4350 (n = 2, 3)	No data
SDSS J130147.97+434549.4	5400 (n = 1 or n = 2)	No data
SDSS J223606.51+291559.9	6450, 4300 (n = 2, 3)	Non-variable

Figure 1.7: *Left:* SDSS spectra of seven candidates close, detached binaries containing magnetic white dwarfs. All of these systems appear to show strong cyclotron features. *Right:* List of the seven candidates close, detached binaries containing magnetic white dwarfs from SDSS spectroscopy and measured wavelengths of the cyclotron harmonics. Both from Parsons et al. (2021a).

If the white dwarf is strongly magnetic, the disk is truncated at the magnetospheric radius of the white dwarf. For field strength of $1 \lesssim B \lesssim 10\,\mathrm{MG}$ the disk is only partly disrupted while for the strongest fields disk formation is fully suppressed ($B \gtrsim 10\,\mathrm{MG}$). In these magnetic systems, known as intermediate polars (truncated disk) or polars (no disk), the overflowing material follows the field lines and is accreted onto the white dwarf magnetic poles. In general, the evolution of cataclysmic variables is dictated by the angular momentum loss and by the internal structure of the companion. There is a high incidence of magnetism in cataclysmic variables ($20 - 40\%$) which is not reflected in the observed fraction of magnetic white dwarf in PCEBs, which are the progenitors of cataclysmic variables (Pala et al., 2020). In general, the magnetic field in cataclysmic variables reaches strengths of several hundreds of MG with an average field strength of $\sim 30\,\mathrm{MG}$ (Schreiber et al., 2022).

Wide white dwarf plus white dwarf

In wide binary systems, stars evolve independently due to significant distances, with the ages and distances determined through the study of non-magnetic companions (Dobbie et al., 2012). In that work, they reveal two new wide double-degenerate binary systems, with three out of four exhibiting nonmagnetic components surpassing typical field white dwarfs in mass. Additionally, three unresolved double-degenerate systems, comprising both magnetic and non-magnetic objects, are documented in the literature (Liebert et al., 1993; Nelan, 2007; Vennes et al., 2009; Bergeron et al., 1993).

White dwarf plus white dwarf (PCEBs)

This type of binary evolved through two phases of mass transfer, and at least one of them has been unstable mass transfer in which a common envelope was created. This resulting double white dwarf system evolves toward shorter periods driven by angular momentum loss and eventually either merges or becomes a semi-detached double white dwarf system (see next paragraph). The only known system that has a strong magnetic white dwarf is NLTT 12758 and a new scenario for magnetic field systems based on Isern et al. (2017a). More details are in Chapter 3. These systems form the objects discussed in this thesis. Neither the common envelope dynamo theory nor the crystallization idea have been tested in the context of detached double white dwarfs.

White dwarf plus white dwarf in a semi-detached configuration (AM CVn)

AM Canum Venaticorum or AM CVn stars are a type of cataclysmic variable. These systems have orbital periods of less than 70 [min.] and the companion white dwarf may be a stripped helium star or a white dwarf with a lower mass than the accretor. Three scenarios have been suggested to explain the formation of AM CVn stars. The first is the systems form from a double white dwarf binary, where the less massive is brought to contact with its Roche lobe because of its orbital shrinking caused by angular momentum loss through gravitational wave radiation. The second is, that the progenitors could be binaries with a white dwarf plus a non-degenerated helium-core burning star. Finally, this system could be the product of a cataclysmic variable with an evolved donor, where the envelope of the donor is completely stripped during the cataclysmic variable phase. In other words, the secondary star is progressively eroded until only the helium-rich nucleus remains and an AM CVn is born Pala et al. (2020). Magnetic white dwarfs in AM CVn are rare. Only two systems, SDSS J080449.49+161624.8 and Gaia14aae, seem to be magnetic but with a relatively weak magnetic field of $10^3 - 10^5$ G.

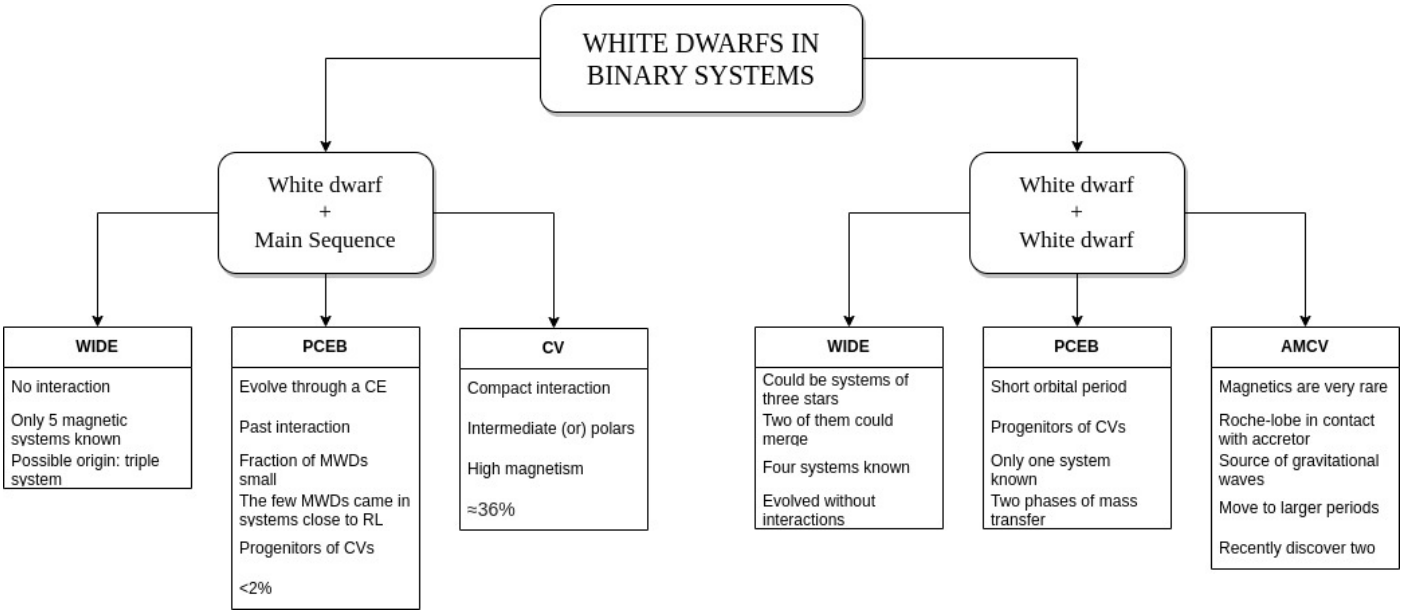

Figure 1.8: This diagram illustrates the various binary systems studied over the years, including those explored in this thesis, classified by the type of companion, and emphasizes their key features.

Chapter 2

Objective and Methodology

As outlined in the introduction, the vast majority of stars end their lives as white dwarfs. The fact that some of these stellar remnants host extremely strong magnetic fields while others do not remains an important puzzle for stellar evolution.

The investigation of strong magnetic field white dwarfs and white dwarf binaries involves numerous theories, but none of them have been able to explain the observed magnetism entirely. Among the currently discussed theories are the common envelope dynamo, the merger of two white dwarfs or degenerate cores of giant stars, and a dynamo driven by crystallization and fast rotation.

Most recent works were dedicated to comparing model predictions with observed samples of single white dwarfs or white dwarfs in close binaries with main sequence star companions. This thesis aims to perform a comparison between the theoretical predictions of different theories for the occurrence of magnetic fields in white dwarfs that are part of double white dwarf binary systems with the currently available observational constraints. By adding another class of objects to the mix, we aim to further progress with our understanding of the origin of magnetic fields in white dwarfs.

To achieve the primary objective of this research, a Python algorithm was developed to generate multiple initial sets of binary systems. These initial data sets were fed into the `BSE` code to simulate the evolution of a large number of systems and to predict the current population of double white dwarfs formed through two common envelope phases. The `BSE` code was modified to make it easier to collect data at the end of the process. In what follows we describe the results of this theoretical exercise but start with a review of the currently available observational information on double white dwarfs.

Chapter 3

Observations of double white dwarf

For over two decades, scientists have recognized that double white dwarf binaries would be a significant source of signals to be detected by space-based gravitational wave observatories. There are expected to exist around 10,000 double white dwarf systems that can be studied in detail using these future gravitational wave detectors (e.g. Nelemans et al., 2001; Ruiter et al., 2010; Korol et al., 2017).

Double white dwarf binaries were first discovered in the late 1980s, primarily featuring low-mass helium-core white dwarfs. These white dwarfs cannot form through single-star evolution within the age of the universe and were initially identified through radial velocity studies (Marsh et al., 1995a). In the past decade, efforts like the Extremely Low-Mass (ELM) white dwarf survey have contributed significantly to this field by targeting specific regions in color-color diagrams occupied by various types of white dwarfs. The ELM survey alone has discovered 98 double white dwarfs so far (Brown et al., 2020a).

Double white dwarfs are not only important as detectable gravitational wave sources but also might help to further understand which mechanism is generating magnetic fields in white dwarfs. Previous works have considered single white dwarfs (Bagnulo and Landstreet, 2021b) or white dwarfs in binaries with main sequence star companion (Schreiber et al., 2021b). Providing new constraints by taking a look at the population of magnetic double white dwarfs represents a natural next step towards a better understanding of the origin of magnetic fields. In this work, I aim to undertake this initiative.

Table 3.1: Parameters of the known close double white dwarfs with measured orbital periods. We ignored many ELM systems where the only component with measured temperature is certainly a helium-core white dwarf. For a comprehensive list of such systems see Brown et al. (2020b).

Name	$M_1[M_\odot]$	$M_2[M_\odot]$	$T_{\rm eff,1}[K]$	$T_{\rm eff,2}[K]$	Period	Reference
NLTT11748 (WD 0342+176)	0.136-0162	**0.707-0.740**	8706±136	**7597±119**†	0.24 day	1
CSS 41177	0.38±0.02	0.32±0.01	24500	11500	2.78 hr	2,3
GALEXJ171708.5+675712	0.185±0.01	≥0.86	14 900±200	–	5.90 hr	4
SDSS J065133.33+284423.3	0.25	0.55	16 400±300	–	12.75 min.	5
SDSS J075141.18-014120.9	0.19±0.02	$0.97^{+0.06}_{-0.01}$	15 750±240	–	1.92 hr	6
SDSS J115219.99+024814.4	**0.47±0.11**	**0.44±0.09**	**25 500±1000**	**14 350±500**	2.40 hr	7, 8
ZTF J153932.16+502738.8	$\mathbf{0.61}^{+0.017}_{-0.022}$	$0.210^{+0.014}_{-0.015}$	**48 900±900**	≤10 000	6.91 min.	9
ZTF J190125.42+530929.5	–	–	28 000±500	17 600±400	40.60 min.	10
ZTF J2243+5242	$0.349^{+0.093}_{-0.074}$	$0.384^{+0.114}_{-0.074}$	$22\,200^{+1800}_{-1600}$	$16\,200^{+1200}_{-1000}$	8.8 min	11
PG 1632+177	$0.392^{+0.069}_{-0.059}$	$\mathbf{0.526}^{+0.095}_{-0.082}$	8 800±500	**11 200±500**	2.05 day	12
WD 1534+503	$0.392^{+0.069}_{-0.059}$	$\mathbf{0.617}^{+0.110}_{-0.096}$	8 900±500	**8 500±500**	0.71 day	12
SDSS J033816.16-813929.9	0.23±0.015	0.38+0.05-0.03	18 100±300	10 000±1000	30.6 min.	13
SDSS J063449.92+380352.2	$\mathbf{0.452}^{+0.070}_{-0.062}$	$0.209^{+0.034}_{-0.021}$	$\mathbf{27\,300}^{+4000}_{-2900}$	$10\,500^{+300}_{-200}$	26.5 min	13
WD 1434+503 (SDSS J143633.29+501026.8)	0.23(01)	–	17 120(200)	–	1.15 hr	14
WD 1050+522 (SDSS J105353.89+520031.0)	0.22(01)	–	16 150(200)	–	0.96 hr	14
SDSSJ1337+3952	**0.46±0.02**	0.26±0.01	**9 450±80**	7 520±170	99 min.	15
WD0028-474	**0.60±0.06**	0.45±0.04	**18 500±500**	17 000±500	9.35 hr	16
SDSSJ0318–0107	. 0.4±0.05	**0.49±0.05**	14 500±500	**13 500±500**	45.9 hr	16
HE0410-1137	**0.51±0.04**	0.39±0.03	**16 000±500**	19 000±500	12.2 hr	16
NLTT12758	**0.83±0.03**	**0.69±0.05**	**7950±50**	**7220±180**	1.154 day	17
WD1202+608 (Feige 55)	**0.3-0.487**	≥0.25	**56 300±1000**	–	1.493 day	18
SDSSJ125733.63+542850.5	0.24	**1.06±0.05**	6400±50	**13 030±150**	4.6 hr	19
WD 1704+481	0.39±0.05	**0.56±0.07**	9000	**10 000**	0.145 day	20, 21
WD0136+768	**0.47**	0.37	**18 500**	10 500	1.41 day	21, 22
WD1704+481	0.39± 0.05	**0.54**	9000	**10 000**	0.145 day	21
WD0957-666	0.37±0.02	0.32±0.03	30000	11 000	1.46 hr	21, 23, 24
WD1204+450	0.46	**0.52**	31 000	**16 000**	1.603 day	21
WD0135-052 (L870-2)	**0.47±0.05**	**0.52±0.05**	**7470±500**	**6920±500**	1.556 day	25, 26
WD1101+364 (=PG1101+364)	0.29	0.33	15 500	12 000	0.145 day	27
PG1115+166	0.70	0.70	–	–	722.2 hr	28
SDSS J174140.49+652638.7	0.17±0.02	≥ 1.11	10540±170	–	1.47 hr	6
WD0225-192 (HE0225-1912)	**0.55**	0.23	**20488**	–	0.22 day	29
WD0315-013 (HE0315-0118)	**0.50**	0.49	**12720**	–	1.91 day	29
WD0320-192 (HE0320-1917)	0.31	0.45	13 248	–	0.86 day	29, 30, 31
WD0326-273	0.364	≥0.96	9158	–	1.88 day	29, 30, 31
WD0453-295	0.40	0.44	16 360	1330	0.36 day	29, 32
WD1013-010	0.32	≥ 0.62	8080	–	0.44 day	29, 30, 31
WD1022+050	0.37	≥0.28	14 693	–	1.16 day	29, 31, 33, 34
HS1102+0934	0.38	≥0.45	16 961	–	0.55 day	29, 30, 31, 35
WD1210+140	0.33	≥0.44	32 127	–	0.64 day	29, 30, 31
HS1334+0701	0.35	–	16 891	–	0.23 day (uncertain)	29
WD1349+144	**0.55**	0.33	**19917**	–	2.21 day	29, 30, 31
HE1414-0848	**0.52**	0.74	**11133**	–	0.52 day	29, 31, 34
HE1511-0448	**0.50**	≥0.67	**50 899**	–	3.22 day	29, 30, 31
WD1824+040	0.4	≥0.73	14 787	–	6.27 day	25, 29, 31, 34
WD2020-425	**0.81**	0.54	**34 004**	–	0.3 day	29, 30
HE2209-1444	0.43	0.72	8471	–	0.28 day	29, 31, 34
WD1428+373	0.35	≥0.23	–	–	1.14 day	34
WD2032+188	0.41	≥0.47	–	–	5.08 day	34
SDSSJ0755+4800	0.42	≥0.90	19 890±350	–	0.55 day	35
SDSSJ1104+0918	0.46	≥0.55	16 710±250	–	0.55 day	35
SDSSJ1557+2823	**0.49**	≥0.43	**12 550±200**	–	0.41 day	35
WD2331+290	0.39	≥0.32	–	–	0.17 day	36
WD1713+332	0.35	≥0.18	–	–	1.12 day	36
WD1241-010	0.31	≥0.37	–	–	3.35 day	36
WD1317+453	0.33	≥0.42	–	–	4.87 day	36
SDSSJ1638+3500	**0.698±0.030**	–	**37250±570**	–	0.91 day	37

† values correspond to assuming a thin envelope. References: (1) Steinfadt et al. (2010), Kaplan et al. (2014), (2) Parsons et al. (2011), (3) Bours et al. (2014), (4) Vennes et al. (2011), (5) Brown et al. (2011), (6) Kilic et al. (2014), (7) Hallakoun et al. (2016), (8) Parsons et al. (2020), (9) Burdge et al. (2019), (10) Coughlin et al. (2020), (11) Burdge et al. (2020), (12) Kilic et al. (2021a), (13) Kilic et al. (2021b), (14) Mullally et al. (2009), (15) Chandra et al. (2021), (16) Rebassa-Mansergas et al. (2017), (17) Kawka et al. (2017a), (18) Holberg et al. (1995), (19) Bours et al. (2015), (20) Maxted et al. (2000) (21) Maxted et al. (2002b) (22) Bergeron et al. (1992), (23) Moran et al. (1997), (24) Bragaglia et al. (1990) (25) Saffer et al. (1988), (26) Bergeron et al. (1989), (27) Marsh (1995), (28) Maxted et al. (2002a), (29) Napiwotzki et al. (2020), (30) Koester et al. (2009), (31) Nelemans et al. (2005), (32) Wesemael et al. (1994), (33) Maxted and Marsh (1999), (34) Morales-Rueda et al. (2005), (35) Brown et al. (2013), (36) Marsh et al. (1995b), (37) Brown et al. (2020b)

Table 3.1 lists various binary systems comprising double white dwarfs that have been subject to observation at distinct research facilities over the preceding years. The parameters provided are the stellar masses of both white dwarfs, their respective effective temperatures, and the orbital period of these binary systems. Components highlighted in bold are (potential) C/O white dwarfs with measured $T_{\rm eff}$ which are the white dwarfs of most relevance for this paper and which are plotted in Figure 3.2.

The data from Table 3.1 was obtained from several papers, with the condition that the orbital period is less than 35 [days] considering all the systems close double white dwarfs. This Table should be complete with respect to the stars that contain a C/O companion with a measured effective temperature. The extremely low-mass white dwarfs are not considered in this table, even after the large number of systems detected (Brown et al., 2020b), because the stellar components with a detected effective temperature are helium-cores which are low-mass stars that are not relevant to understanding the dynamo driven by crystallization and fast rotation. The only exception considered in this study is SDSS J1638+3500, given its status as the most massive system in the study conducted by Brown et al. (2020b). This system is also featured in Figure 3.2.

Figure 3.1 illustrates all the systems listed in Table 3.1 presenting masses of the primary and secondary star, including their errors, in the axes y and x, respectively.

Figure 3.2 illustrates various double white dwarf systems that have been observed using a diverse array of telescopes and instruments. The axes of this diagram represent the stellar mass (M_{WD}) in solar masses ($M_{\odot}$) against the effective temperature (T_{eff}) in Kelvin (K). Notably, the lower-left region of the plot is characterized by a concentration of stars exhibiting effective temperatures ranging from $9,000$K to $30,000$K, with the majority having masses predominantly below $0.65\,M_{\odot}$.

Of particular interest, two data points are highlighted within the plot. These data points correspond to the NLTT 12758 system, which comprises a magnetic white dwarf (DAP) with a hydrogen rich companion white dwarf (DA). This white dwarf is the currently only known magnetic white dwarf that forms part of a close double white dwarf. In the following chapters, we will analyze whether this paucity of magnetic white dwarfs in close double white dwarf binaries can be understood in the context of the mechanisms proposed for magnetic field generation in white dwarfs. The generation of magnetic fields is intrinsically related to the formation and evolution of double white dwarfs. We therefore continue in the next section with a review of currently considered formation scenarios for double white dwarfs.

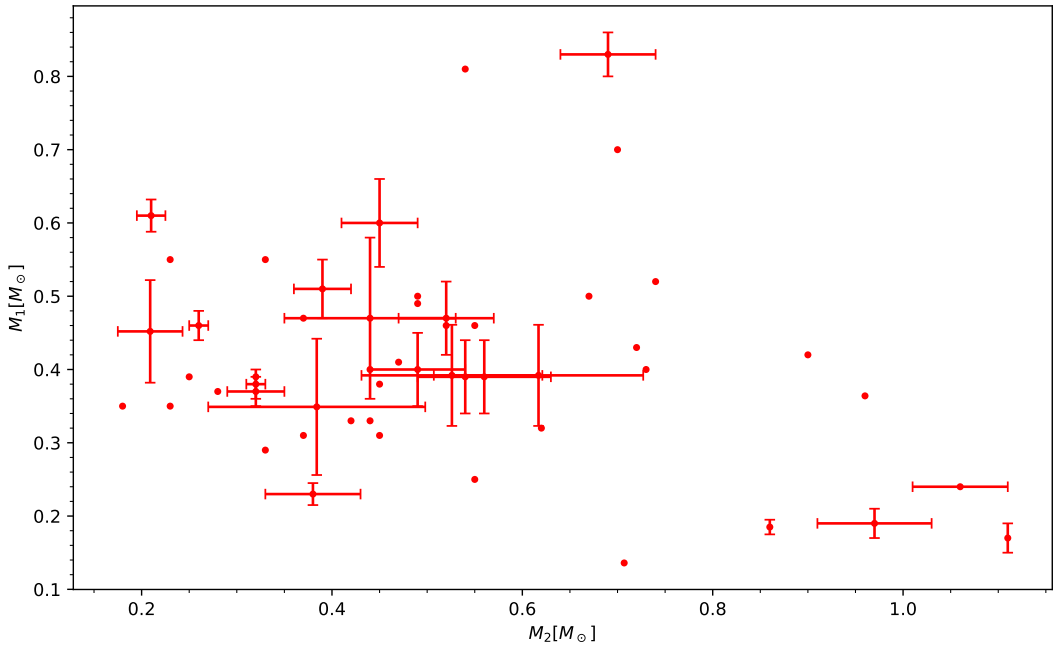

Figure 3.1: This plot shows info from Table 3.1, featuring systems studied in various sources. It reflects the connection between the masses of the primary and secondary stars. The sources are marked in red, with their respective errors.

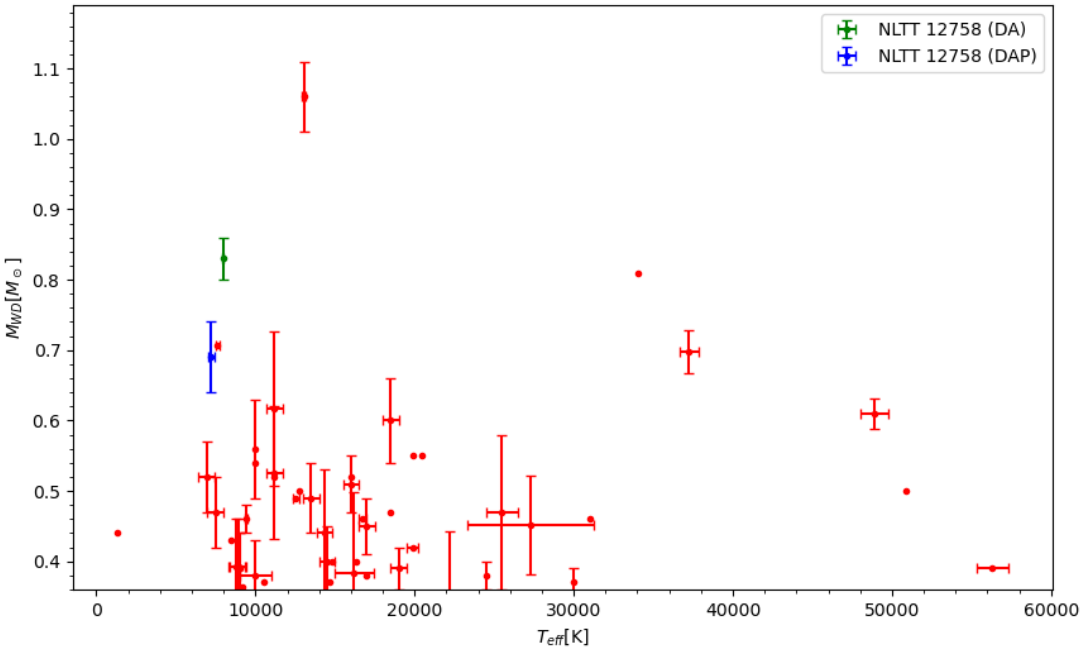

Figure 3.2: Masses and temperatures of the white dwarfs that form part of double white dwarfs listed in Table 3.1. NLTT 12758, which is a system that will be analyzed in Chapter 7 in detail, is highlighted.

Chapter 4

The predicted population of double white dwarfs formed through two common envelopes

As outlined in the introduction, the formation of close double white dwarfs is not yet fully understood. It is clear that two mass transfer phases are required but different combinations of stable and unstable mass transfer (which leads to common envelope evolution) are possible. Analyzing the impact of all possible channels on the different ideas for the generation of magnetic fields is beyond the scope of this thesis.

As a first step towards understanding the formation of double white dwarfs and the generation of magnetic fields, we analyze one evolutionary channel in detail (two common envelope phases) and ignore for now double white dwarf formation through a combination of common envelope evolution and stable mass transfer. The formation through two common envelope phases is frequently considered the most important formation channel of double white dwarfs and, in addition, it is the easiest channel to simulate.

4.1 The Binary Star Evolution (BSE) code

To simulate the formation of double white dwarfs and to perform binary population synthesis we used the Binary Star Evolution code (BSE). This code is an open-source algorithm built to study the formation and evolution of binary systems. BSE, written in fortran, and among its strengths are the fact that it only takes a few seconds to calculate the evolution of a proposed system and that the general evolution is directly shown on the screen. From https://astronomy.swin.edu.au/~jhurley/ the compressed file bse.tar.gz can be downloaded, this file contains the program and the instructions for installation. In addition, there is a link to the main article of the program

(Hurley et al., 2002a), and a live version of the code that uses a simple interface to evolve a binary system with some information about how the program works.

`BSE` uses the tidal interaction to model in detail the circularization of eccentric orbits and the synchronization of stellar rotation with the orbital motion. It also considers gravitational radiation and magnetic braking to model the angular momentum loss. The code also calculates the mass transfer rate when one of the stars fills its Roche lobe. This mass transfer may proceed on a nuclear, thermal, or dynamical time scale. Furthermore, setting different orbital parameters, `BSE` allows for wind accretion, that is, the secondary may accrete some of the material lost from the primary in a wind. More information about the determination of the type and rate of mass transfer, the secondary accretion mechanisms, and the outcome of any merger events can be found in Hurley et al. (2002a).

In order to run the code, after extraction and compilation, an input file must be created or modified to set the initial parameters. The structure of this file is shown in Table 4.1. Each of the elements is set with default values explained in Table 4.2. After the code is executed, a summary of the evolution is printed on the console. This output contains the evolutionary history of the binary stars. Ten columns display the evolutionary time, the mass of the first star, the mass of the companion, the stellar type of the star (detailed in Table 4.3), and the companion, separation, eccentricity, radius for the first and the companion star (in Roche lobe units) and finally, the stage of the evolution. The complete result of the evolution can be found in the output file `binary.dat`.

mass1	mass2	tphys	tb	kstar1	kstar2	z	ecc
neta	bwind	hewind	alpha1	lambda			
ceflag	tflag	ifflag	wdflag	bhflag	nsflag	mxns	idum
pts1	pts2	pts3					
sigma	beta	xi	acc2	epsnov	eddfac	gamma	

Table 4.1: Structure of the input file. The definition, units, and default values of each element are explained in Table 4.2.

The main aim of this thesis is to simulate populations of double white dwarfs and to compare these predicted populations with the sample of observed double white dwarfs. However, before we describe simulated populations, we review the different evolutionary channels showing examples of the formation of double white dwarfs as simulated with `BSE`.

mass1 and *mass2* must be given in solar units. *tphysf* is the maximum evolution time in Myr. *tb* is the orbital period in days. *kstar* is the stellar type: 0 or 1 on the ZAMS - unless in evolved states. z is metallicity in the range $0.0001 \rightarrow 0.03$ where 0.02 is Population I. *eccentricity* can be anywhere in the range $0.0 \rightarrow 1.0$. *neta* is the Reimers mass-loss coefficent ($neta \cdot 4 \times 10^{-13}$: 0.5 normally). *bwind* is the binary enhanced mass loss parameter (inactive for single). *hewind* is a helium star mass loss factor (1.0 normally). *alpha1* is the common-envelope efficiency parameter (1.0). *lambda* is the binding energy factor for common envelope evolution (0.5). *ceflag* > 0 activates spin-energy correction in common-envelope (0). *ceflag* $= 3$ activates the de Kool common-envelope model (0). *tflag* > 0 activates tidal circularization (1). *ifflag* > 0 uses WD IFMR of HPE, (Han et al., 1995b) (0). *wdflag* > 0 uses modified-Mestel cooling for white dwarfs (0). *bhflag* > 0 allows velocity kick at BH formation (0). *nsflag* > 0 takes NS/BH mass from (Belczynski et al., 2002) (1). *mxns* is the maximum NS mass (1.8, nsflag=0; 3.0, nsflag=1). *idum* is the random number seed used by the kick routine.

Table 4.2: Information about the input parameters in the `BSE`.

0	deeply or fully convective low mass MS star
1	Main Sequence star
2	Hertzsprung Gap
3	First Giant Branch
4	Core Helium-Burning
5	First Asymptotic Giant Branch
6	Second Asymptotic Giant Branch
7	Main Sequence Naked helium star
8	Hertzsprung Gap Naked helium star
9	Giant Branch Naked helium star
10	Helium White Dwarf
11	Carbon/Oxygen White Dwarf
12	Oxygen/Neon White Dwarf
13	Neutron Star
14	Black Hole
15	Massless Supernova

Table 4.3: Type of stars type described by `BSE`.

4.2 The evolution of individual systems

As mentioned in the first chapter, white dwarfs are remnants of more massive stars. The specific type of white dwarf that remains depends on the initial mass of the progenitor star and whether it is part of a binary system. In what follows we describe the detailed evolutionary pathways leading to close double white dwarfs formed through two common envelope phases.

The most frequently fully characterized observed type of double white dwarfs are those composed of two helium-core white dwarfs. Both progenitor stars in this type of binary fill their Roche lobe before igniting He in their nuclei. The left part of Figure 4.1 illustrates this process. After 3 Gyr, the primary has filled its Roche lobe when it has already evolved to the first giant branch. At this point, the mass transfer is unstable because of the deep convective envelope. During common envelope evolution, this envelope is expelled at the expense of orbital energy and the core of the donor star transforms into a helium-core white dwarf with a mass of 0.31 $M_{\odot}$. Finally, after 4 Gyrs, when the first white dwarf has already cooled to lower temperatures, the secondary fills its Roche lobe also on the first giant branch, unstable mass transfer starts again and forms a common envelope during which the orbital period further shrinks. The remaining binary star consists of two helium-core white dwarfs.

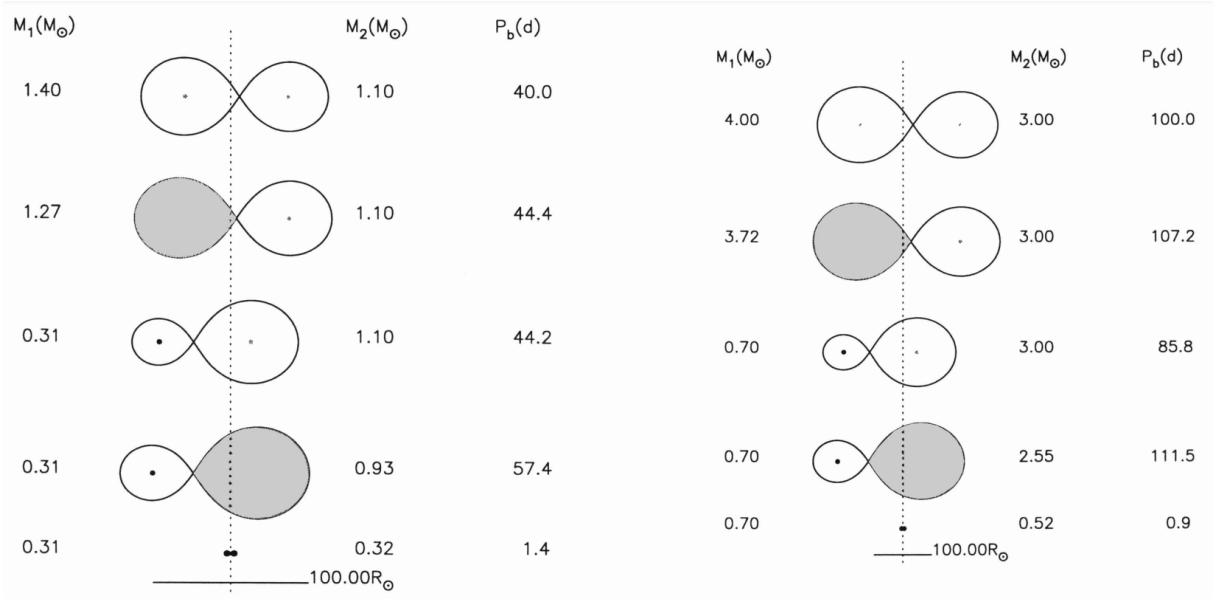

Figure 4.1: Evolutionary scenarios for the formation of a double helium white dwarf (left) and a double C/O white dwarf (right). Credit to Nelemans et al. (2001).

Additionally, there are binary systems consisting of two C/O white dwarfs. These stars form from initially wider systems and both stars interact later in their evolution when the donor star has reached the asymptotic giant branch (AGB). A less common evolutionary path involves more massive stars where the first stage following common envelope evolution is a helium star that

subsequently evolves into a C/O white dwarf.

In the case of systems with a C/O white dwarf and a helium white dwarf, using the model of two common envelopes, the more massive star evolves first and produces the C/O white dwarf, that is, fills its Roche lobe on the AGB. The reduced orbital separation can then cause the second star to fill its Roche lobe on the first giant branch which generates a common envelope phase that leaves behind a helium-core white dwarf.

Binary systems with a white dwarf made of Oxygen-Neon (O/Ne) are not common because this type of star requires the progenitor stars with initial masses of almost $8M_{\odot}$. Such large masses are intrinsically less common than lower mass stars and in addition, the possibility of surviving through two common envelopes without merging is very low.

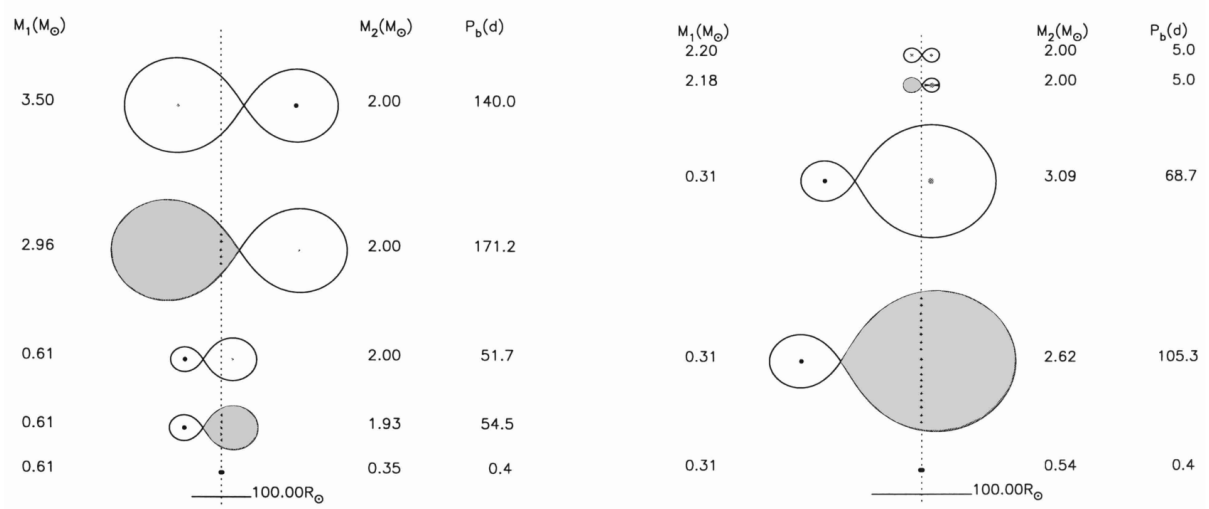

Figure 4.2: Evolutionary scenarios for the formation of CO+He (left) and He+CO (right) pairs. Credit to Nelemans et al. (2001)

In what follows we show the evolution of the radius for both stars for the just discussed different cases. The evolution depicted in Figure 4.3 leads to the formation of two helium-core white dwarfs. When the radius of the first star (magenta) increases (i.e. when the star is on the giant branch), mass transfer between both stars causes common envelope evolution and the core of the giant does not reach the critical mass to star helium-burning. The radius drastically decreases when the envelope is expelled. The same occurs with the second star (cyan) which was initially less massive evolves: it fills its Roche lobe on the first giant branch when the core is still made of helium. Given that mass transfer is dynamically unstable, common envelope evolution is triggered and the two stars spiral-in towards the center of mass once again. The left panel of Figure 4.3 shows the behavior of the orbital period while both stars evolve. The first decay represents the first common envelope between the stars which made them get close, at this point the mass transfer takes control of the situation, and then, when the second star evolves off the main sequence, a second common

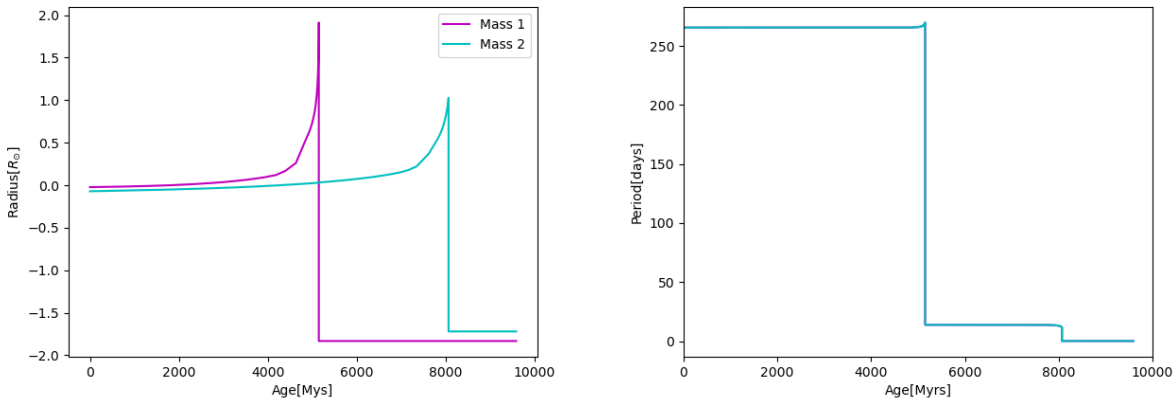

Figure 4.3: Binary evolution of a system consisting initially of two stars with masses of 1.17 $M_\odot$ and 1.10 $M_\odot$. The final masses of the two helium-core white dwarfs are 0.472 $M_\odot$ and 0.268$M_\odot$. The initial period in this system is 265.536 [days], and at the end, the final period is 0.145 [days]. The left plot shows the radius evolution of the stars. The right shows the orbital period evolution of the stars, where the first decay shows the first common envelope and the second decay illustrates the second common envelope.

envelope phase occurs, which makes the two stars to get even closer. At this point, both of the stars are white dwarfs and a double helium-core white dwarf has formed.

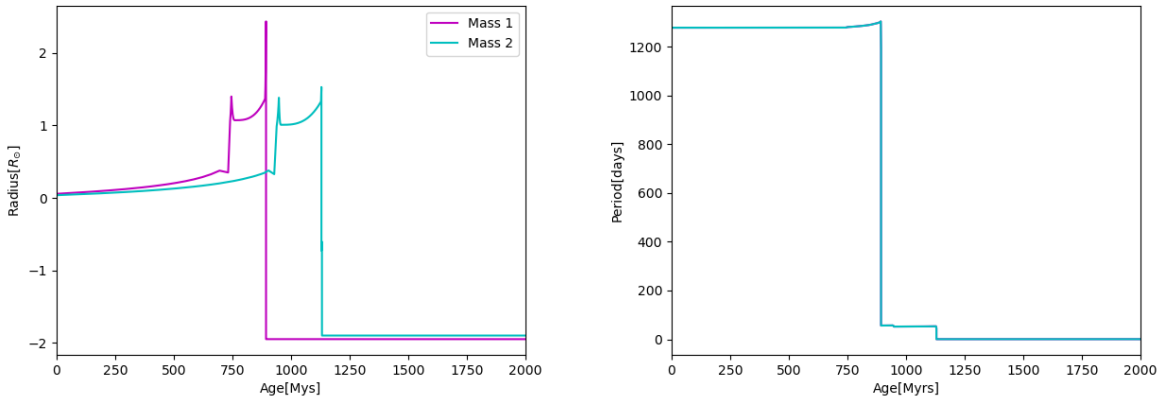

Figure 4.4: Initial masses of 2.059 $M_\odot$ and 1.881 $M_\odot$ of a main sequence binary evolving into a binary consisting of two C/O core white dwarfs with masses of 0.720 $M_\odot$ and 0.611 $M_\odot$. The initial period of the binary is 1277.816 [days] and the final period in the system is 0.628 [days]. The orbital period was chosen so that both stars fill their Roche lobe on the AGB. The white dwarf that forms first is more massive than the white dwarf formed in the second common envelope phase. The left plot shows the evolution of the stellar radii while the right plot shows the evolution of the orbital period.

In Figure 4.4, the left plot shows the formation of a double white dwarf consisting of two

C/O core white dwarfs. Both stars do not fill their Roche lobe on the RGB phase and reach core helium-burning. During the latter, the radius of the star decreases. At the end of core helium-burning, the stars reach the AGB but only when the radius on the AGB exceeds the maximum radius reached during RGB evolution, the stars fill their Roche lobes.

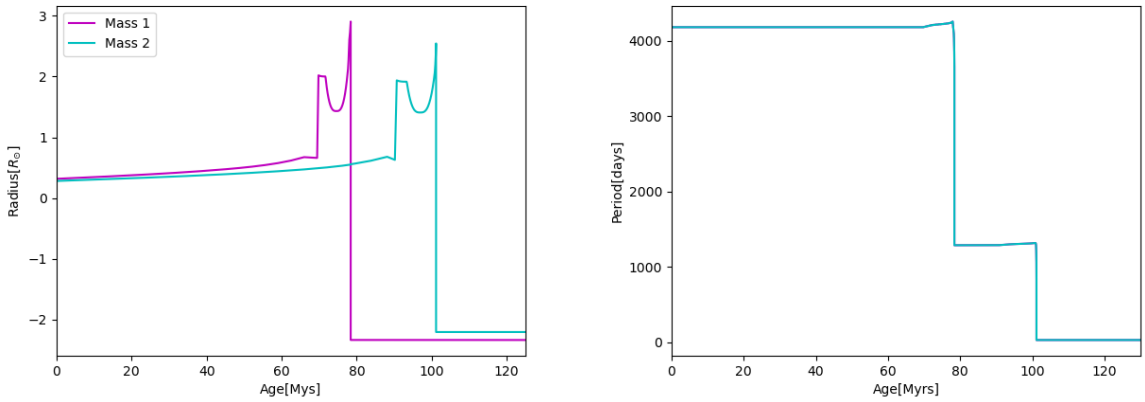

Figure 4.5: This system contains two stars with initial masses of $5.734\,M_\odot$ and $5.017\,M_\odot$ and final masses as a white dwarf of $1.276\,M_\odot$ and $1.154\,M_\odot$. The initial period of this system is 4183.169 [days] and the final period is 31.082 [days]. Both stars are O/Ne type which is massive and a rare type of system, and the mass between them is not too different, which can be seen in the right plot where the second common envelope occurs, in the orbital period and is notorious for this interaction, unlike the plots above.

Figure 4.5 shows the formation of a binary system consisting of two O/Ne white dwarfs. This type of white dwarf is more massive than the other ones and very rare. In this case, the star evolves off the main sequence, entering the RGB phase, and the radius increases until it reaches the first peak which corresponds to the ignition of core helium-burning. The radius of the star shrinks during core helium-burning and common envelope evolution only starts when helium in the core gets exhausted, and the star moves up the AGB. Core masses of $1.2 - 1.4\,M_\odot$ can lead to carbon-burning, and, consequently, all the carbon in the core is converted to oxygen and neon. The left panel shows the radius evolution of both stars and the right panel shows the behavior of the orbital period because of the two common envelope phases.

Figure 4.6 illustrates the formation of a binary system composed of an O/Ne and a He core white dwarf. Here, the first star evolves through the main sequence, the RGB, helium-core burning, and large parts of the AGB before filling its Roche lobe at the end of the AGB. The second (less massive) star fills its Roche lobe on the RGB before core helium-burning and therefore a helium-core white dwarf is formed.

As the last example, we show in Figure 4.7 the formation of a white dwarf binary consisting of an O/Ne core white dwarf with a C/O core white dwarf companion. The initially more massive star

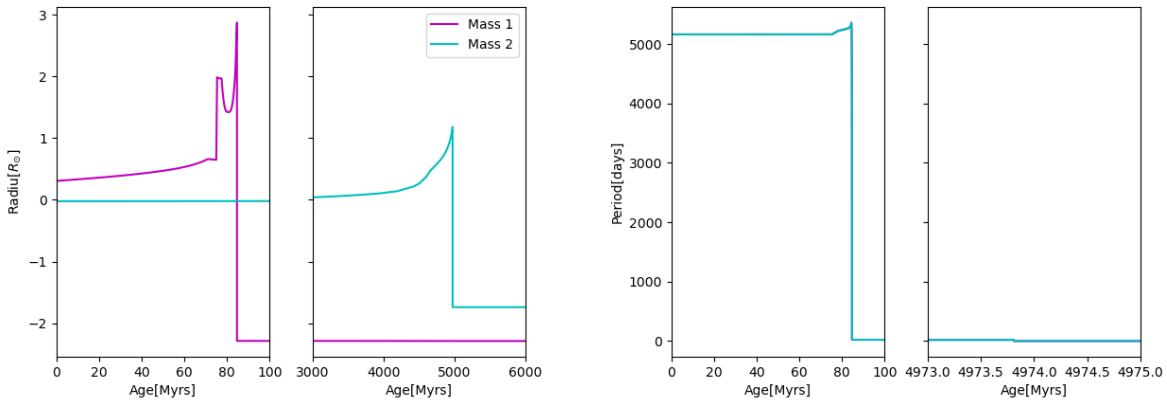

Figure 4.6: This plot represents the evolution of a binary system of two white dwarfs, an O/Ne and a He, which have initial masses of $5.519\,M_\odot$ and $1.082\,M_\odot$ and final masses of $1.241\,M_\odot$ and $0.300\,M_\odot$. The initial period of the system is 5163.731 [days] and the final period is 0.653 [days]. The left plot shows the rapid evolution of the more massive star which was on the AGB when common envelope evolution was triggered by unstable mass transfer. The companion of this star is a less massive star that fills its Roche lobe during the first giant branch. The right panel shows the evolution of the stellar radii while the left plot shows the behavior of the orbital period as a consequence of the interaction between both stars.

fills its Roche lobe late on the AGB which triggers the first common envelope phase. The second star also reaches the AGB but fills its Roche lobe before carbon-burning starts and consequently, the second white dwarf that is formed is made of C/O.

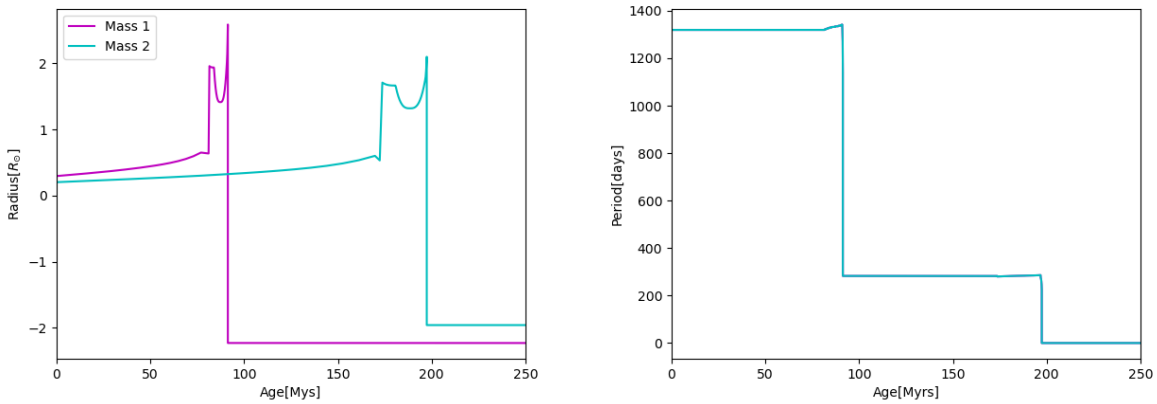

Figure 4.7: This plot shows the binary system consisting of an O/Ne and C/O white dwarf, the first one more massive than the second one, having initial masses of 5.307 $M_\odot$ and 3.722 $M_\odot$ and final masses as white dwarf of 1.183 $M_\odot$ and 0.739$M_\odot$. The initial period of the binary is 1320.063 [days] and the final period is 0.199 [days]. The first star, which is more massive, evolves through the main sequence reaching the RGB where the He starts to burn, then passes through the AGB phase burning C/O mostly, and finally O/Ne because of its high mass. The second star evolves similarly to the first one, but because its mass is not high enough, only burns C/O and then stops the evolution leaving a C/O white dwarf. The left plot shows the behavior of the orbital period through both interactions of the stars, the first common envelope is more notorious because the first star is more massive and the second one, but both interactions are visible.

4.3 Evolving large numbers of binaries with BSE

In this thesis, a representative sample of binary stars was evolved with the BSE code to compare the observed sample of double white dwarfs with predicted populations of systems that formed through two common envelopes. For this purpose, some modifications were needed, constraints in different input parameters were performed and the development of new scripts was required as explained in detail in what follows.

Due to the short execution time of the BSE code, this tool allows the simulation of a large number of binary systems to study populations and distributions. To accomplish this in an efficient form, the input file was removed to reduce reading time. Most of the input values were fixed inside the code (see Table 4.4), while others (*mass1*, *mass2*, *tphys* and *tb*) were configured to be set on the console when the program is called for execution. Regarding the common envelope efficiency parameter *alpha* (α) and the binding energy factor (α_{rec}), these values were fixed for specific sets of systems and modified to study their influence on the predicted population (used values in Section 5.1).

kstar1	1	**kstar2**	1	**z**	0.001	**ecc**	0.0
neta	0.5	**bwind**	0.0	**hewind**	1.0	**ceflag**	0
tflag	1	**ifflag**	0	**wdflag**	1	**bhflag**	0
nsflag	1	**mxns**	3.0	**idum**	29769	**pts1**	0.05
pts2	0.01	**pts3**	0.02	**sigma**	190.0	**beta**	0.125
xi	1.0	**acc2**	1.5	**epsnov**	0.001	**eddfac**	10.0
gamma	-1.0						

Table 4.4: Input parameters fixed in the `BSE` code.

4.4 Analysis of initial populations

Once the `BSE` code was altered to read input parameters from the command shell, some `PYTHON` scripts were developed.

The first code creates a sample of start-up binary systems for further processing in `BSE` code. A diagram of this code is in Figure 4.8. In this script, a function is defined to create a set of N random masses for the first star. Then, the code assigns upper and lower limits for these primary star masses and uses the initial mass function (IMF) $1.0 < M_1/M_\odot$ from Kroupa et al. (1993) to constrain the final values of the first mass from all binary systems. Limits are defined to cover the range between 1 to 8 $M_\odot$. The IMF (defined as $M_1^{-2.7}$) is compared with a random value of the mass. If the IMF is greater than the random value, the code assigns this value to the mass of the primary star and then continues, otherwise new values are created until the condition is fulfilled for each star. Subsequently, this code creates the mass of the companion following the mass ratio $q = \frac{M_2}{M_1}$ where q is a random number between 0 and 1. The next condition to be satisfied for these systems is that only secondary masses greater than 0.8 are allowed to be assigned for the companion.

The separation of each system is estimated using restricted aleatory values (R_1, R_2) following Davis et al. (2008) criteria for separation:

$$S_i = (10000\, R_1 + 3)/695700 \tag{4.1}$$

$$S_f = 0.078636/S_i \tag{4.2}$$

If $S_f > R_2$ the value S_f is assigned as the final separation.

The period follows Kepler's third law:

$$P = \sqrt{\frac{4\pi^2 S_f^3}{G(M_1 + M_2)}} \tag{4.3}$$

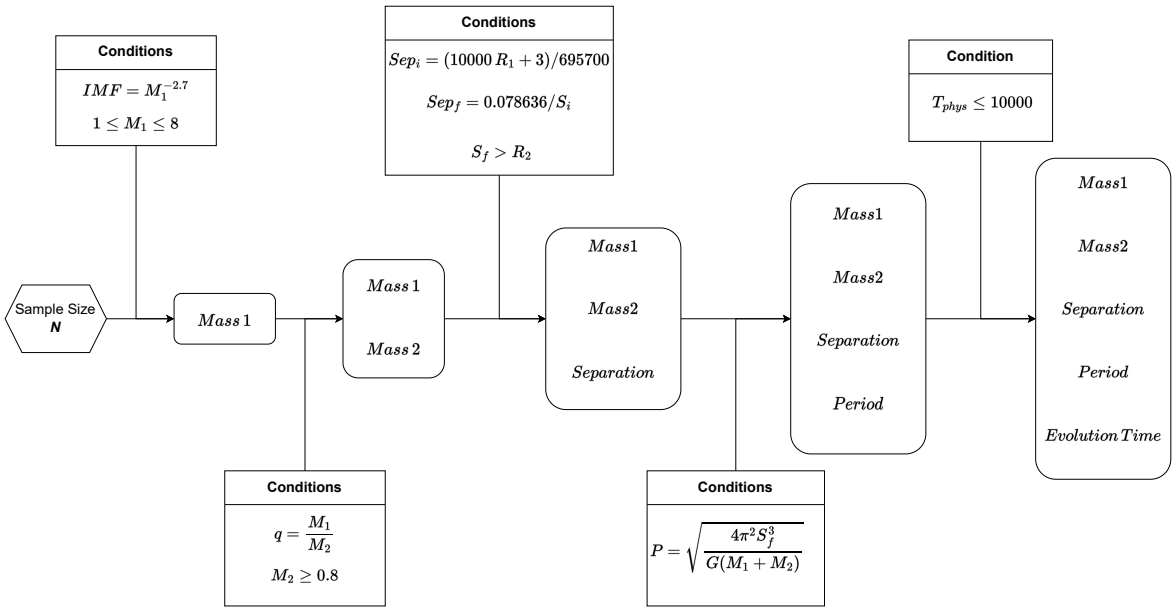

Figure 4.8: This diagram represents the process after the `BSE` is excecuted.

Finally, the evolutionary time for the `BSE` code is set up to a limit of $10,000$ Gyr (the age of the Galaxy), and each star has been assigned a birth time according to a constant star formation rate. The evolutionary time is thus simply the difference between the moment of birth and 10 Gyr. This set of parameters, representing N binary systems, are stored in a simple text file that can be called with another script as the initial input for `BSE` code.

After establishing the initial parameters, an examination is conducted using various histograms to ensure they follow the correct relationships within the Initial Mass Function (IMF) for the primary mass, the q-distribution, and the orbital period distribution.

The next (and main) script, reads the text file containing the input parameters and calls the `BSE` code for each of the systems written in that file. Then, the code creates a folder to store the incoming results (outputs) of the program. Finally, the program selects the systems that during their evolution have achieved two common envelopes and end with two white dwarfs.

4.5 Binary Population Synthesis

Initial distributions were obtained by setting up parameters as described in Section 4.4, verifying that the histograms are consistent with the initial distributions provided in Zorotovic et al. (2014a). Figure 4.9 provides evidence that the primary star's mass distributions align with the normalized initial mass function from Kroupa et al. (1993), while the secondary mass is constrained by the q-value and mass limits. Throughout the formulation of the initial parameters, the histogram of

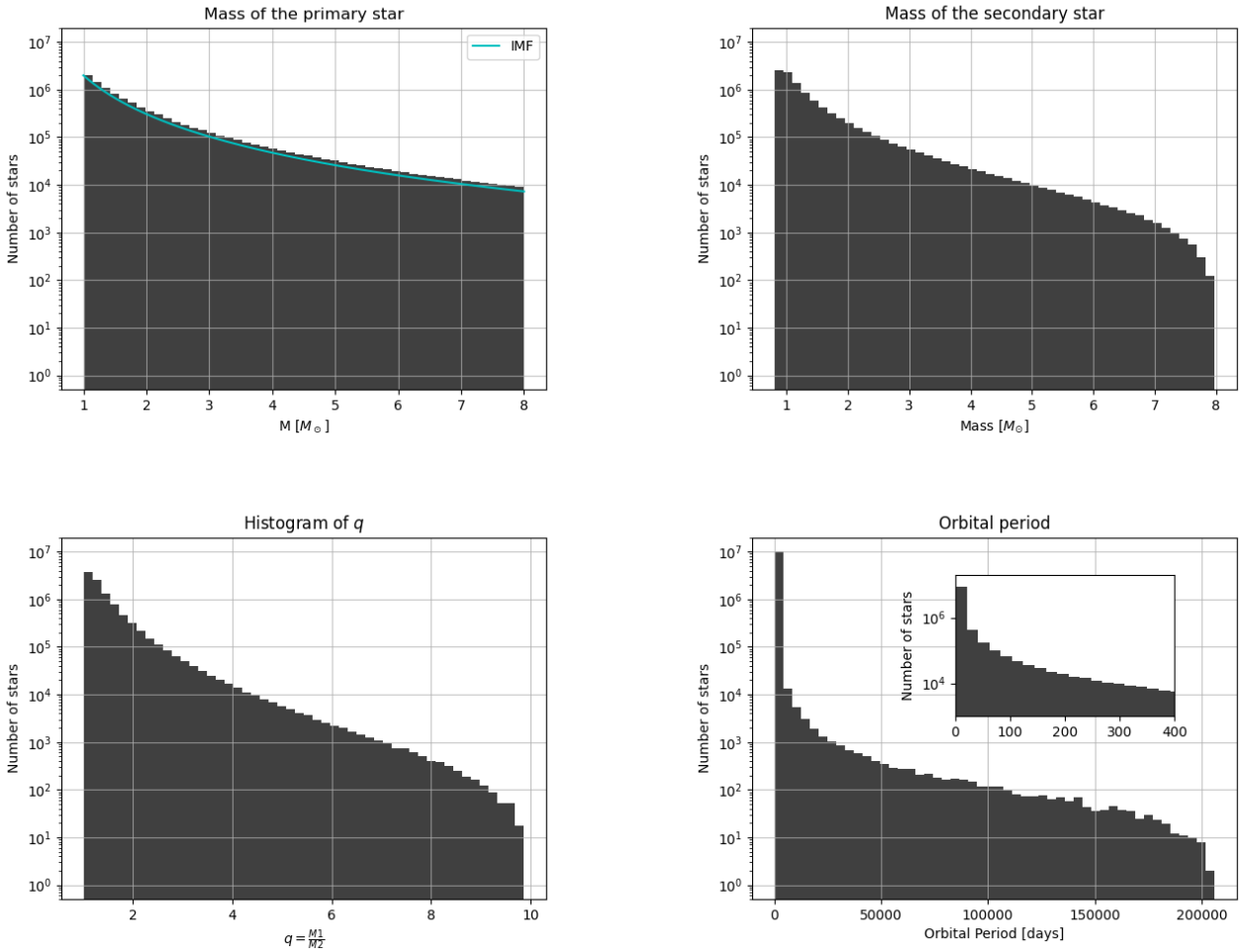

Figure 4.9: Example of the histograms obtained from a sample of 10^7 binary systems. The upper-left diagram proves that the mass distribution of the primary star (black) follows the normalized initial mass function (cyan). The mass distribution of the secondary star is shown in the upper-right panel. The lower-left panel displays the histogram of final values of q which is not flat because of the mass filter process. In the lower-right panel is the distribution of the orbital period.

q initially exhibits a flat distribution, which changes when the lower limit for the secondary mass, $M_2 > 0.8\,M_\odot$, is imposed as can be seen in the Figure 4.9. The initial orbital separation follows the distribution presented in Davis et al. (2008) and then uses the Equation 4.3 (Keplers third law) to determine the orbital period distribution presented in Figure 4.9 featuring a subplot that zooms in on the initial segment, revealing that the majority of systems exhibits periods shorter than 100 [days].

Figure 4.10 shows the different binary populations that can be obtained from the `BSE` and also uses the software created to constrain the populations to the limits needed, like initial masses or separations. This differentiation between these populations depends on the need to obtain populations, for example, where one of the stars in the binary is a supernova or both stars are

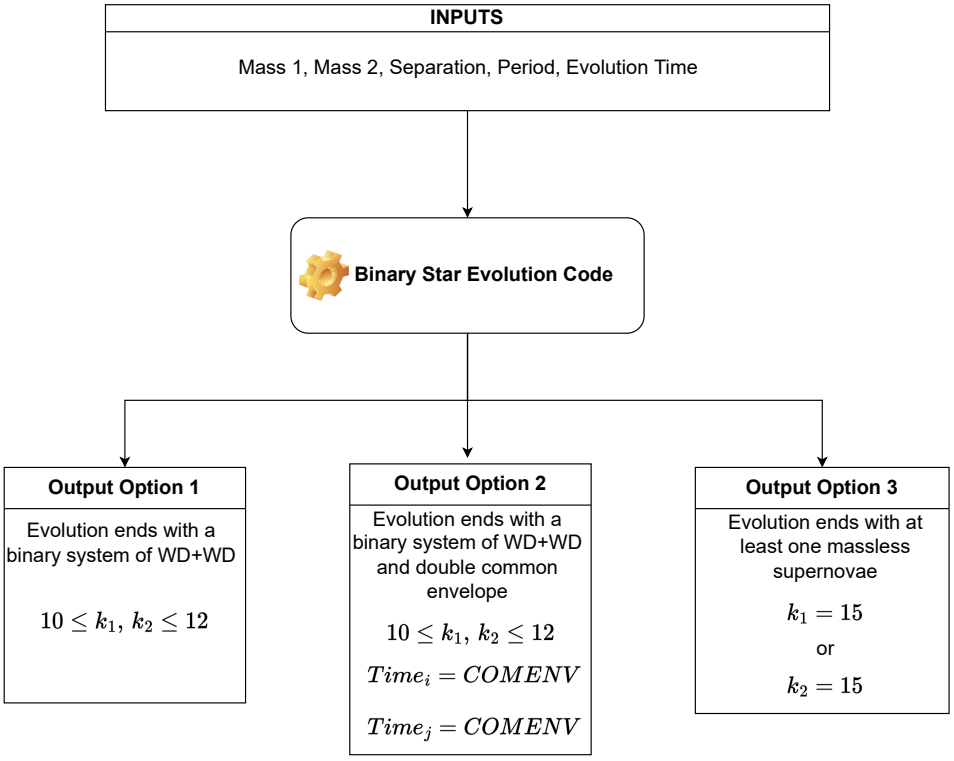

Figure 4.10: The diagram shows first the input which enters the BSE and then the three options created at this work to obtain different results including the ones used in this thesis.

white dwarfs. All options can start with the same input created by mass 1, mass 2, and separations which are used to obtain the period and the maximum evolution time.

Chapter 5

Magnetic fields generated by the common envelope dynamo

Magnetic fields present in some white dwarfs have been difficult to understand since they have been found in limited surveys and in different types of systems (single white dwarfs, white dwarfs in close detached binaries, and white dwarfs in close semi-detached binary stars). Current models for the generation of strong magnetic fields include the fossil field (Braithwaite and Spruit, 2004), the double degenerate merger (García-Berro et al., 2012), and the common envelope dynamo scenarios (Tout et al., 2008).

In the previous sections, we have described in detail how binary population synthesis can be performed for double white dwarf forming through two common envelope phases. The main aim of this thesis, however, is to constrain the origin of magnetic fields in white dwarfs using information on close double white dwarfs. In this section, we combine our population synthesis with the first scenario for the origin of magnetic fields that we would like to test: the generation of strong magnetic fields during common envelope evolution.

5.1 Magnetic Field generation during common envelope evolution

According to the common envelope dynamo idea, a magnetic dynamo, either similar to stellar dynamos which require convection, or the dynamos that are supposed to drive viscosity in accretion disks, is generated during the common envelope phase. In the event that a giant star fills its Roche lobe, unstable mass transfer may occur, potentially resulting in a state where the giant envelope engulfs both its own core and its companion star. The companion could be either a non-evolved low-mass main sequence star or an already-formed white dwarf. The stars inside the envelope

are expected to spiral inward towards their common center of mass while energy and angular momentum from their orbit is transferred to the common envelope, leading to its gradual ejection. At the beginning of mass transfer, an accretion disk forms around the accreting star. Accretion disks are differentially rotating and subject to magneto-rotational instability (Balbus and Hawley, 1991). As the cores approach each other, their orbital period decreases, resulting in differential rotation within the common envelope. The significant size of the common envelope is anticipated to lead to a substantial level of convection (giant envelopes are typically convective anyway).

While detailed magneto-hydrodynamical simulations of common envelope evolution have not been performed yet (probably because this is really difficult), the occurrence of differential rotation and convection offers the potential to generate strong magnetic fields either through a convective dynamo or through the magneto-rotational instability. It is then assumed that this magnetic field can penetrate the non-degenerate surface of the core and subsequently freeze as the core cools and contracts. The proximity of the cores at the end of the common envelope evolution results in a much faster differential rotation within the common envelope. As a consequence, the frozen magnetic field is assumed to be stronger if the final orbital period of the binary is smaller (Tout et al., 2008).

To estimate the magnetic fields of a white dwarf formed through common envelope evolution we used the equation of Briggs et al. (2018):

$$B = 1.35 \times 10^{10} \left(\frac{\Omega}{\Omega_{crit}} \right) [G] \tag{5.1}$$

where Ω is the orbital angular velocity just after the common envelope evolution given by,

$$\Omega = \frac{2\pi}{P_{orb}} yr^{-1} \tag{5.2}$$

where P_{orb} is the orbital period just after the common envelope and Ω_{crit} is the break-up angular velocity of the white dwarf given by

$$\Omega_{crit} = \sqrt{\frac{GM_{WD}}{R_{WD}^3}} = 2\pi \sqrt{\left(\frac{M_{WD}}{M_\odot} \right) \left(\frac{R_{WD}}{AU} \right)^{-3}} yr^{-1} \tag{5.3}$$

R_{WD} is,

$$R_{WD} = 0.0112 R_\odot \sqrt{\left(\frac{M_{Ch}}{M_{WD}} \right)^{2/3} - \left(\frac{M_{WD}}{M_{Ch}} \right)^{2/3}} \tag{5.4}$$

where $M_{Ch} = 1.44\, M_\odot$ and M_{WD} is the white dwarf mass (Briggs et al., 2018).

5.2 Mass and magnetic field

Having at hand a binary population model and a simple equation relating the magnetic field strength to the final orbital period of the binary star, we can now predict a population of double white dwarfs formed through two common envelopes including the magnetic field strengths of the white dwarfs.

More specifically: we started with 10^7 initial systems and then proceeded to select "Output Option 2" as illustrated in Figure 4.10. Subsequently, we extracted the mass, period, and radius values of the resulting systems from the output files. Using the equations described in the previous section, we calculated the magnetic fields in mega-gauss. This entire process was repeated three times, with different combinations of the common envelope efficiencies, that is α (0.3 and 1.0) and α_{rec} (0.0 and 0.1).

Figure 5.1 displays different outcomes for double white dwarf systems, depending on the combinations of α and α_{rec}. Specifically, the first plot from the left corresponds to $\alpha = 0.3$ and $\alpha_{rec} = 0.0$, the center plot to $\alpha = 1.0$ and $\alpha_{rec} = 0.0$, and the last one to $\alpha = 1.0$ and $\alpha_{rec} = 0.1$. The first set of parameters corresponds to a case assuming that a relatively small fraction of the available orbital energy is used to expel the envelope (30%) and that the recombination energy stored in the envelope does not contribute. These assumptions seem to explain reasonably well the characteristics of the observed population of post common envelope binary stars (Zorotovic et al., 2010). The second set of parameters assumes an efficient use of orbital energy and again no contributions from recombination energy. These values are frequently used when supernovae Ia rates are calculated from binary population models (Toonen et al., 2012). Finally, we assume that recombination energy contributes which seems to be required to explain some individual systems such as IK Peg (Zorotovic et al., 2010), KOI-3278 (Zorotovic et al., 2014b), and WD 1856+534 (Lagos et al., 2021)

In addition to presenting the magnetic fields calculated using Briggs's equation, as indicated by the color bar, Figure 5.1 shows the observational sources from Table 3.1 but only considers the masses without the magnetic field. These plots reveal that for the predicted white dwarfs, more massive objects exhibit lower magnetic fields, while less massive stars have stronger magnetic fields. Another observation is that the number of double white dwarf systems with at least one magnetic star increases when the parameter combinations change. Comparing these simulation results to the observations listed in Table 3.1 and plotted in Figure 5.1, we find that the simulations yield a significantly larger relative number of objects with massive white dwarfs, especially in the right-hand plot, with $\alpha_{rec} = 1.0$ and $\alpha = 0.1$. However, the combination of $\alpha_{rec} = 0.0$ and $\alpha = 0.3$ in the left-hand plot predicts fewer systems to survive, and the fraction of helium core white dwarfs in the predicted population is larger which agrees better with the observations. However,

even in this case, the observed masses are not well reproduced by the simulations. This indicates, independent of the predicted magnetic field strength, that most currently known double white dwarfs most likely did not form through two common envelope phases.

Figure 5.2 presents three plots that depict the relationship between magnetic field strength and orbital period for varying combinations of α and α_{rec}. The left-hand plot corresponds to $\alpha = 0.3$ and $\alpha_{rec} = 0.0$, the center plot to $\alpha = 1.0$ and $\alpha_{rec} = 0.0$, and the right-hand plot to $\alpha = 1.0$ and $\alpha_{rec} = 0.1$. Notably, these plots reveal that as the orbital period increases, the magnetic fields decrease. This prediction of binary systems with closer orbits having stronger magnetic fields cannot be seen in the observations. In particular, none of the observed helium-core white dwarfs has a detected magnetic field. The model, however, predicts the opposite. Even if most double white dwarfs formed through one common envelope phase and one phase of stable mass transfer (which is indicated by the comparison of the masses), the common envelope dynamo idea would predict far too many strongly magnetic white dwarfs. We can therefore exclude the common envelope dynamo (in its current form) to play a significant role in the generation of white dwarf magnetic fields.

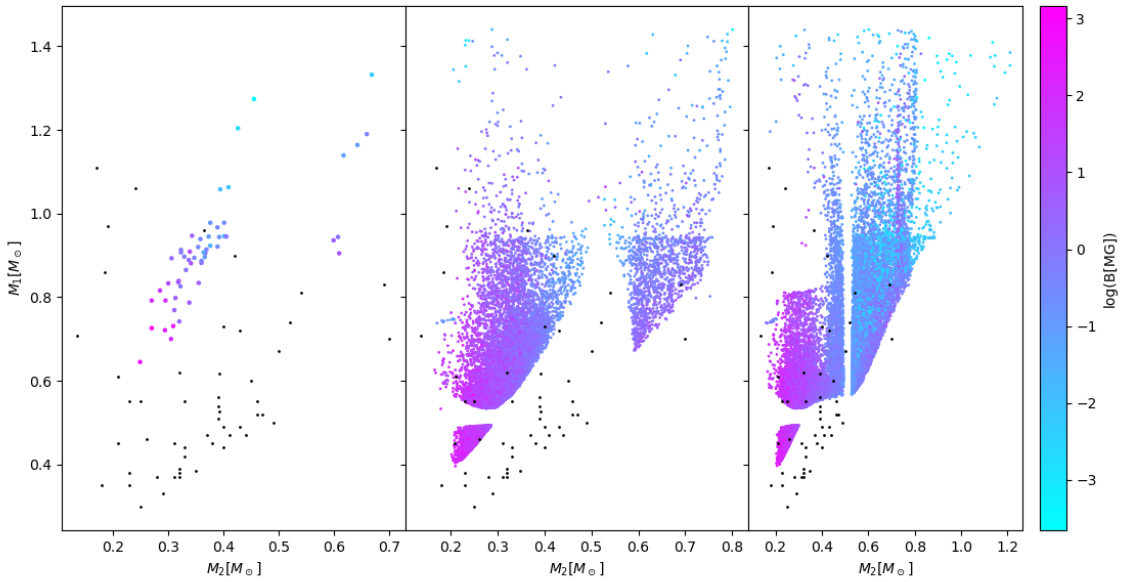

Figure 5.1: The three plots shows the results of the `BSE`, with mass 1 versus mass 2 in solar masses, and are also combined with the results of the magnetic fields (in MG) associated with these masses represented by a colorbar showing the different intensities of the magnetic field. Also, in each plot, there are the observations, in black, listed in the Table 3.1. The left-hand plot corresponds to $\alpha = 0.3$ and $\alpha_{rec} = 0.0$, the center plot to $\alpha = 1.0$ and $\alpha_{rec} = 0.0$, and the right-hand plot to $\alpha = 1.0$ and $\alpha_{rec} = 0.1$.

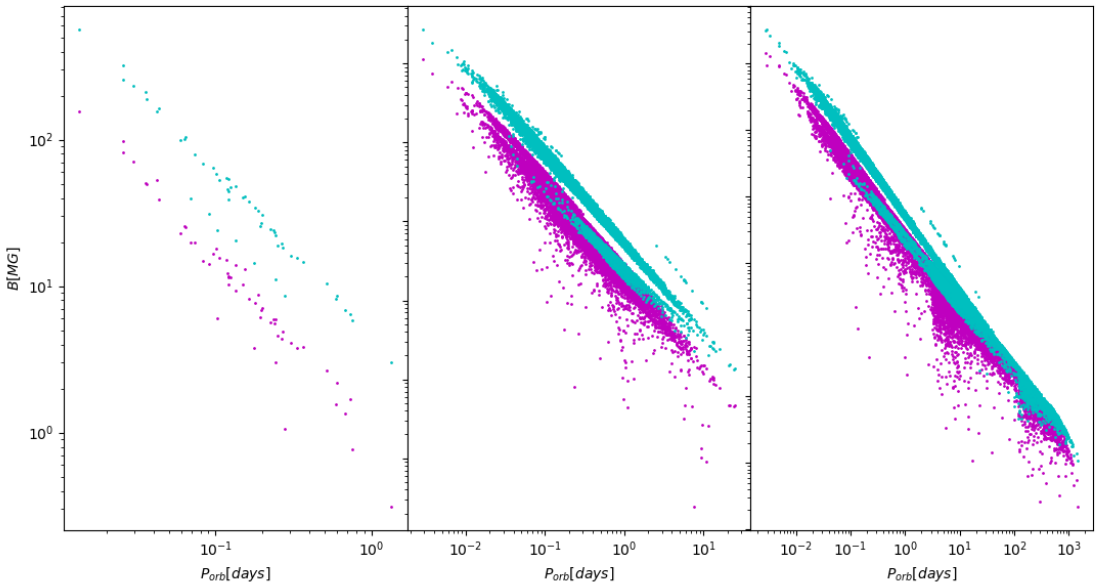

Figure 5.2: The three plots show the magnetic field (in MG) versus orbital period (in days) changing the α and α_{rec}. The two colors (magenta and cyan) represent the two masses of the binary, mass 1 and mass 2 respectively. The left-hand plot corresponds to $\alpha = 0.3$ and $\alpha_{rec} = 0.0$, the center plot to $\alpha = 1.0$ and $\alpha_{rec} = 0.0$, and the right-hand plot to $\alpha = 1.0$ and $\alpha_{rec} = 0.1$.

Chapter 6

Testing the crystallization and rotation driven dynamo

The second scenario suggested for the generation of magnetic fields in white dwarfs we test in this thesis is a dynamo driven by fast rotation and crystallization of the core of C/O white dwarfs. This scenario has received a lot of attention in recent years because observations of single white dwarfs as well as white dwarfs in binaries indicate that strong fields typically appear in old white dwarfs that have cooled down for $2-3\,\mathrm{Gyr}$ (Parsons et al., 2021b; Bagnulo and Landstreet, 2021b). In what follows we summarize the basic idea of magnetic field generation through the crystallization and fast rotation driven dynamo before we compare the predictions of our binary population model with the observations.

6.1 Magnetic Field generation though the rotation and crystallization driven dynamo

The scenario proposed by Schreiber et al. (2021a), follows the idea of Isern et al. (2017a), which suggests that the magnetic field of white dwarfs could be generated by a mechanism similar to that of low-mass stars or planets. As a white dwarf with a C/O core cools, the ions in the core begin to freeze in a lattice structure. During this crystallization process, the chemical potential, temperature, and pressure of the liquid and solid phases must remain in equilibrium. As a consequence, in crystallizing white dwarfs the solid phase becomes richer in oxygen and sinks while the carbon excess mixes with the outer liquid envelope which is redistributed by Rayleigh–Taylor instabilities. This configuration is similar to that found in the core of the Earth, where the light element release associated with the inner core growth is a primary driver of the dynamo generating the Earth's magnetic field Lister and Buffett (1995).

The idea of generating strong magnetic fields through this dynamo led Schreiber et al. (2021b) to develop a new evolutionary scenario for close white dwarf binaries. Initially, the white dwarf emerged from common envelope evolution without being strongly magnetic. Once the mass transfer starts, these systems become cataclysmic variables and accrete mass and angular momentum. If the spun-up white dwarf has cooled enough to contain a crystallizing core, its structure will consist of an outer convective zone of carbon and a solid inner core of oxygen (Schreiber et al., 2022) and generate a magnetic field.

Using the energy scaling law to estimate the strength of the generated magnetic field, however, Isern et al. (2017b) showed that field strengths exceeding 1 MG can be excluded. Schreiber et al. (2021b) argued that a possible dependence on the magnetic Prandtl number is missing in the energy scaling law and the generation of strong fields can therefore not be excluded. Very recently, Ginzburg et al. (2022) argued that the convective turn-over time is much larger than assumed by Isern et al. (2017a) which would implies that white dwarfs are almost always in the fast rotation regime. Combining this finding with a scaling law based on the balance between the Lorentz and Coriolis forces (super-equipartition) even permits the generation of strong magnetic fields (reaching 100 MG) without postulating a magnetic field enhancement due to the white dwarf's Prandtl number. In the absence of a detailed model for the dynamo in white dwarfs, we here assume that the recently proposed magnetic dynamo requires relatively rapid rotation and a crystallizing core to generate strong magnetic fields in white dwarfs.

The second criterion for the dynamo to work is that the core of the white dwarf must have started to crystallize. The onset of crystallization depends on the temperature and the white dwarf mass. The currently available cooling tracks that include crystallization differ slightly in the predicted temperatures for the onset of crystallization. There are two models of onset for crystallization, those by Bédard et al. (2020a) and Salaris et al. (2010a).

The crystallization onset information provided by Salaris et al. (2010b) is derived from a stellar evolution database known as BaSTI (Bag of Stellar Tracks and Isochrones). On the other hand, Bédard et al. (2020b) determined the onset of crystallization using data from the available SDSS white dwarf catalogs up to DR12. They analyzed 1806 hot white dwarfs and utilized the Modules for Experiments in Stellar Astrophysics (`MESA`) to generate initial models for their study. This work incorporated the latest generation of model atmospheres and theoretical cooling tracks, both appropriated for hot white dwarfs. We use both criteria in this work which illustrates the involved uncertainties.

6.2 Comparison with observational data

In Figure 6.1, we conduct a comparison between the onset of crystallization as predicted by the models presented in the works of Salaris et al. (2010b) and Bédard et al. (2020b) with the positions of all C/O white dwarfs found in close double white dwarf systems, whose mass and effective temperature are known.

The observed parameters of the magnetic white dwarf component within NLTT 12758 (highlighted in blue in Figure 6.1) are in accordance with the presence of a crystallizing core in the white dwarf. Thus, the rotation and crystallization driven dynamo mechanism provides a plausible explanation for its magnetic characteristics. Most other white dwarfs within close double white dwarf systems are either helium-core white dwarfs, for which the dynamo scenario does not apply, or they are too hot to have crystallizing cores. The fact that these white dwarfs are not magnetic is thus consistent with the dynamo theory for magnetic field generation in white dwarfs. Nevertheless, among the limited number of double white dwarfs containing C/O white dwarfs, three additional systems have cooled sufficiently to enter the crystallization phase. Apart from the magnetic (DAP) white dwarf in NLTT 12758, components close to or beyond the onset of crystallization are its higher mass non-magnetic (DA) companion and the more massive white dwarfs in SDSS J125733.63+542850.5 (hereafter SDSS J1257+5428) and NLTT 11748 (the white dwarfs highlighted with cyan and magenta in Figure 6.1).

6.3 Comparison with simulated data

As we have just shown, the observations of double white dwarfs fit relatively well with the predictions of the rotation and crystallization driven dynamo. In what follows we evaluate how the observed population compares with the binary population predicted to have formed through two common envelope phases. In Figure 6.2 we show the two cooling tracks of Salaris et al. (2010b) and Bédard et al. (2020b), and the predicted systems of double white dwarfs. The cyan points refer to the white dwarf that formed second which will very likely dominate an observed spectrum (because it is younger and less massive). The fraction of these white dwarfs that should be magnetic (i.e. older than the onset of crystallization) is significantly larger for more efficient common envelope evolution. For the lowest common envelope efficiency (0.3), we predict only a single one of these white dwarfs, as is observed. If common envelope evolution is inefficient, it might be that the double white dwarfs that form through this channel contain a cool magnetic and massive component but that this component is not observed because the younger and brighter low-mass white dwarf companion dominates the spectrum.

In contrast, we can exclude the combination of efficient common envelope evolution and the

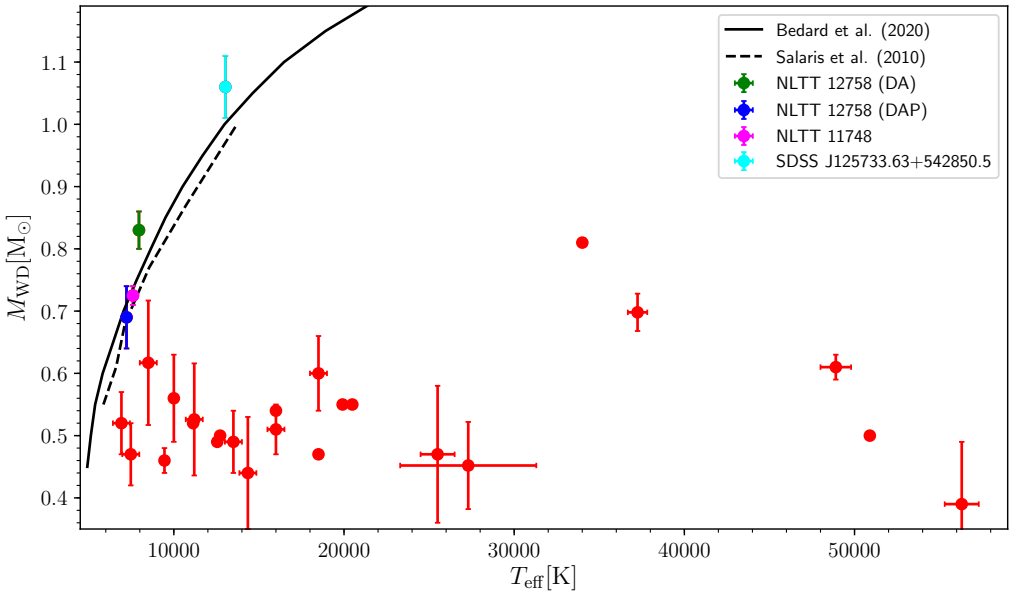

Figure 6.1: Comparison of the mass and effective temperature of the known white dwarfs that form part of a close (period less than 35[days]) double white dwarf (from Table 3.1) with the onset of crystallization according to the cooling sequences by Salaris et al. (2010b, black dashed line) and Bédard et al. (2020b, black solid line). The vast majority of the white dwarfs are too hot to be crystallizing. Among the few exceptions is the magnetic component in NLTT 12758. For this white dwarf, the measured parameters are consistent with crystallization in its core. In addition, the spin period has been measured to be very short (23 [min.]) it appears plausible that the rotation and crystallization driven dynamo generated the strong magnetic field. Three more white dwarfs are also consistent with having a crystallizing core. This might indicate that those white dwarfs, in contrast to the magnetic component in NLTT 12758, did not accrete angular momentum during their evolutionary history or that their magnetic field has not been detected yet.

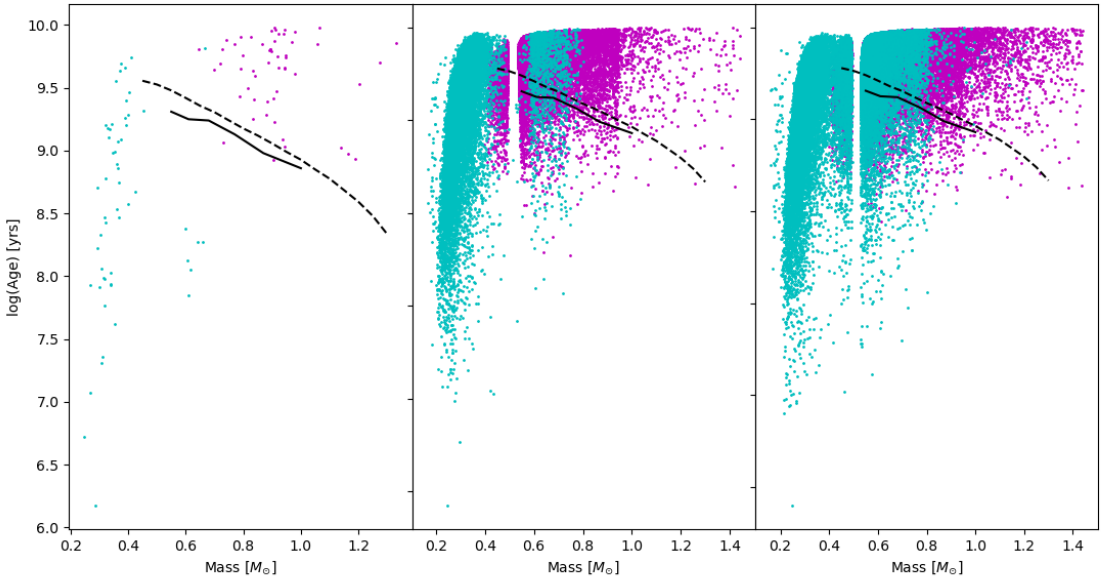

Figure 6.2: The three plots, left hand $\alpha = 0.3$ and $\alpha_{rec} = 0.0$, the center $\alpha = 1.0$ and $\alpha_{rec} = 0.0$, and the right hand $\alpha = 1.0$ and $\alpha_{rec} = 0.1$, shows the behavior of the simulated data with respect with the two cooling tracks of Salaris et al. (2010b) and Bédard et al. (2020b).

dynamo to correctly predict the occurrence rate of magnetism in double white dwarfs. In this case, the model predicts a relatively large number of crystallizing double white dwarfs resulting from the first common envelope phase.

Finally, we note that the disagreement between the predicted and observed white dwarf masses of course remains (the simulations are identical to those presented in the previous one). This clearly implies that two common envelope phases are not the main channel for the observed double white dwarfs. It seems more likely that a combination of common envelope evolution and stable mass transfer formed the majority of the observed systems. In the next chapter, we will evaluate the latter option to understand the evolutionary history of the only double white dwarf that contains a magnetic component: NLTT 12758.

Chapter 7

NLTT 12758 Evolution

At present, only one close double white dwarf system is known to host a strongly magnetized white dwarf, NLTT 12758. This system consists of a magnetic white dwarf and an apparently non-magnetic white dwarf companion. The non-magnetic hydrogen-rich (DA) white dwarf is more massive ($M = 0.83 \pm 0.03\,M_{\odot}$) than the magnetic (DAP) companion ($M = 0.69 \pm 0.05\,M_{\odot}$), the orbital period of the binary is 1.154 [days], the spin period of the magnetic white dwarf has been measured to be 23 [min.], and the cooling ages of both white dwarfs are comparable (Kawka et al., 2017a). The recently proposed magnetic dynamo requires relatively rapid rotation and a crystallizing core to generate strong magnetic fields in white dwarfs. However, there are some other white dwarfs that could be magnetic according to the dynamo while only in NLTT 12758 a strong magnetic field has been detected. If the hypothesis that the fast rotation and crystallization driven dynamo generated the magnetic field in NLTT 12758 is correct, the other white dwarfs with crystallizing cores must either not have sufficiently spun up during their formation or maybe strong magnetic fields have not been detected yet. To understand the magnetic field generation in close double white dwarfs the evolutionary history of NLTT 12758 must be understood to be able to consider potential evolutionary differences.

The evolutionary scenario of NLTT 12758 has been suggested to consist of two consecutive common envelopes (Kawka et al., 2017b). The reconstruction of both common envelopes (Zorotovic et al., 2010, 2014b) concludes that the two common envelopes scenario is possible with the inclusion of an additional energy source (Schreiber et al., 2022). Using the two common envelopes evolution scenario, then the more massive white dwarf should be formed in the first stage of the common envelope and the less massive in the second common envelope. As the spiral-in process reduces the orbital separation, the initially less massive cannot evolve further up the giant branches than the first one.

As we have seen in the previous sections, additional energy is unlikely to contribute significantly to expelling the envelope. Moreover, there is still the question of why the magnetic white dwarf

is rotating fast. Because of these open questions, there is a doubt that maybe the evolution is different.

The approach that relies on two common envelopes and employs the classical energy budget equation encounters difficulties when attempting to account for numerous double white dwarf systems. Therefore, a γ algorithm was suggested which is based on the conservation of angular momentum. Although, this algorithm tends to hide the problem instead of solving it. An alternative form of evolution considers that the first mass transfer should be stable and non-conservative, this occurs when the mass rate of both progenitors stars is close to one (Ge et al., 2020).

The fact that both cooling ages are similar (2.2 ± 0.2 and $1.9 \pm 0.4\,\mathrm{Gyr}$) could indicate that the history of the formation of the system was in fact different. In this case, if both progenitors evolved off the Main Sequence at the same time, both initial masses must have been similar and hence the first mass transfer could have been stable.

Using the open-source 1D stellar evolution code `MESA`, an attempt was made to replicate the evolutionary pathway leading to NLTT 12758. The investigation revealed that the magnetic white dwarf in this system emerged as a result of a stable, non-conservative mass transfer process. Consequently, it was determined that the mass of the ZAMS progenitor must have been approximately $\simeq 3.60\,M_{\odot}$ or greater. This occurs because the mass increase of the primary white dwarf is interrupted when it becomes an asymptotic giant branch star and fills its Roche lobe. This implies that the first white dwarf progenitor cannot be much more massive than $\sim 4.0\,M_{\odot}$ because the core mass at the onset of Roche lobe overflow must be comparable with the value observed in the magnetic white dwarf companion in NLTT 12758.

To reproduce the mass of the magnetic white dwarf and to have a stable mass transfer, the red giant (Figure 7.1) must be on the early asymptotic giant branch. On the other hand, to reproduce the mass of the non-magnetic white dwarf, its progenitor needs to increase before the onset of common envelope evolution. This implies that when the non-conservative mass transfer ends, the orbital period has to be between $\sim 3,500 - 4,000\,[\mathrm{days}]$, which requires that the initial orbital period for the ZAMS binary cannot be less than $\sim 500\,[\mathrm{days}]$. The limits for this orbital period depend on the accretion efficiency during stable mass transfer. To have this, when the donor is an early asymptotic giant branch star, we found that the accretion efficiency must be less than ~ 0.5 which means that at least half of the mass that leaves the early asymptotic giant branch donor is not accreted by the donor but leaves the binary.

The best-fitting model in this approach, combining dynamically stable non-conservative mass transfer followed by a phase of dynamically unstable mass transfer is illustrated in Figure 7.1. The ZAMS stars initially possess masses of $3.85\,M_{\odot}$ and $3.50\,M_{\odot}$ and are in an orbital configuration with a period of $670\,[\mathrm{days}]$. During the mass transfer process, the less massive white dwarf is formed, with the initially less massive secondary star attaining a mass of $4.49\,M_{\odot}$ and an orbital

period extension to 3814 [days].

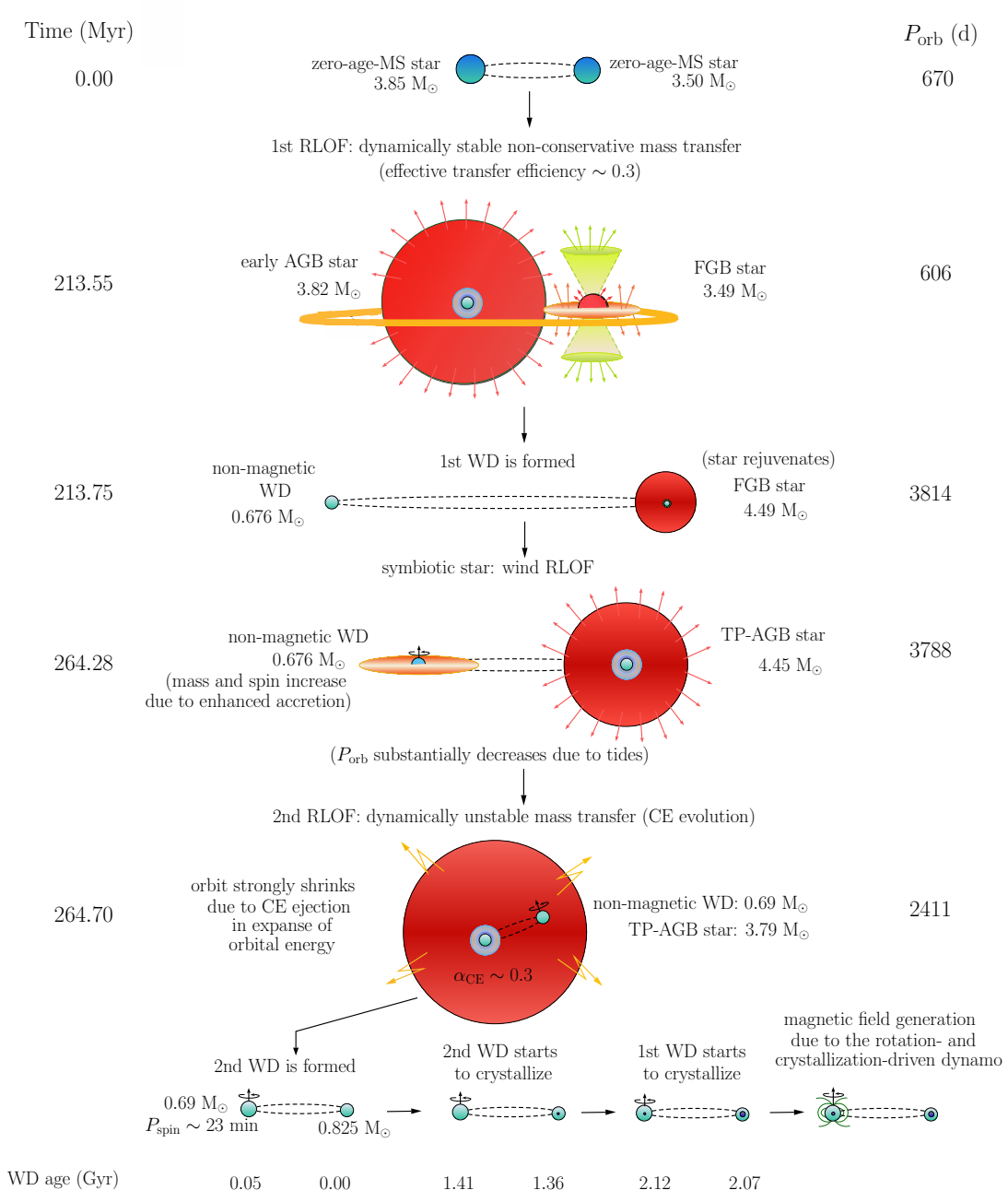

Figure 7.1: The revised evolutionary scenario for NLTT 12758 consists of stable mass transfer followed by a symbiotic phase and common envelope evolution after which the orbital period is similar to the one we observe today. According to this scenario, the less massive white dwarf forms first and accretes mass and angular momentum during the second mass transfer phase. When this fast-spinning white dwarf starts to crystallize, the dynamo mechanism suggested by Schreiber et al. (2021b) generates the strong magnetic field that has been detected by Kawka et al. (2017a).

Upon evolution into a Thermally Pulsing Asymptotic Giant Branch (TP-AGB) star, the binary

system transforms into a symbiotic star. The white dwarf within the system begins to accrete mass and angular momentum from the stellar wind, causing it to spin up and ultimately reach observed mass values ($0.69\,M_{\odot}$) and a spin period of approximately ~ 23 [min.]. The influence of tidal forces during this phase results in a reduction of the orbital period.

The evolution of both stars prior to the final common envelope phase is further illustrated in Figures 7.2 and 7.3. In the figures, are plotted the core masses, orbital periods, mass transfer rate, and spin period as a function of the mass of the initially less massive star. In Figure 7.2 the left panel shows the mass of the white dwarf that later forms the magnetic one, the white dwarf that forms first, increases between two principal transfer mass events due to the wind accretion (red dashed-dotted line). The core mass of the initially less massive star (blue line) has already reached more than $0.4\,M_{\odot}$ when the stable mass transfer begins but also it increases after the mass transfer ends until the system enters the common envelope evolution.

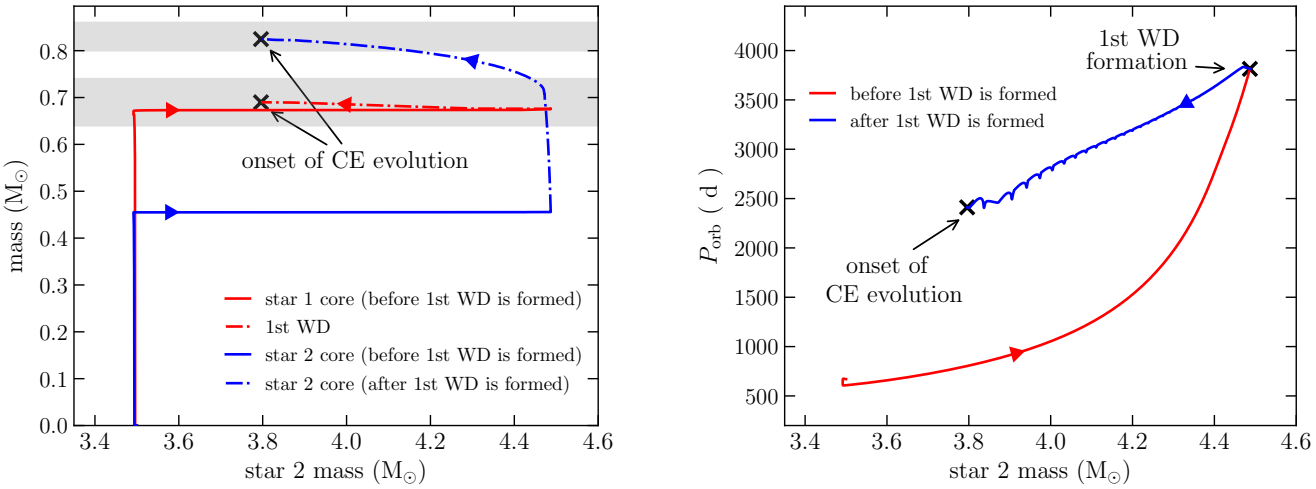

Figure 7.2: Evolution with the DA progenitor (star 2) mass of some properties of the best-fitting model for NLTT 12758, prior to the onset of the common envelope phase, namely star core and first white dwarf masses (left-hand panel) and orbital period (right-hand panel). The range of DA and DAP white dwarf masses, as inferred from observations, are indicated as gray areas in the left-hand panel. We reasonably well reproduce those properties in our modeling with the `MESA` code.

The right panel in Figure 7.2 shows how the orbital period changes during its evolution. While the stable mass transfer phase is on, the period increases (red line) but decreases before the onset of the common envelope evolution because of the tidal forces when the less massive star initially evolves in the AGB.

In Figure 7.3 the left panel shows the mass transfer evolution. The red line shows that the stable mass transfer reaches values of $\sim 10^{-3}\,M_{\odot}yr^{-1}$, and that roughly one-third of the wind

mass loss rate (blue) is accreted by the white dwarf (green) during the symbiotic phase. This accretion mass leads to the spin-up of the white dwarf that formed first as displayed in the left panel. Finally, the right panel shows that the spin period depends on the mass transfer rate and on the spin-up efficiency and is in very good agreement with the observations.

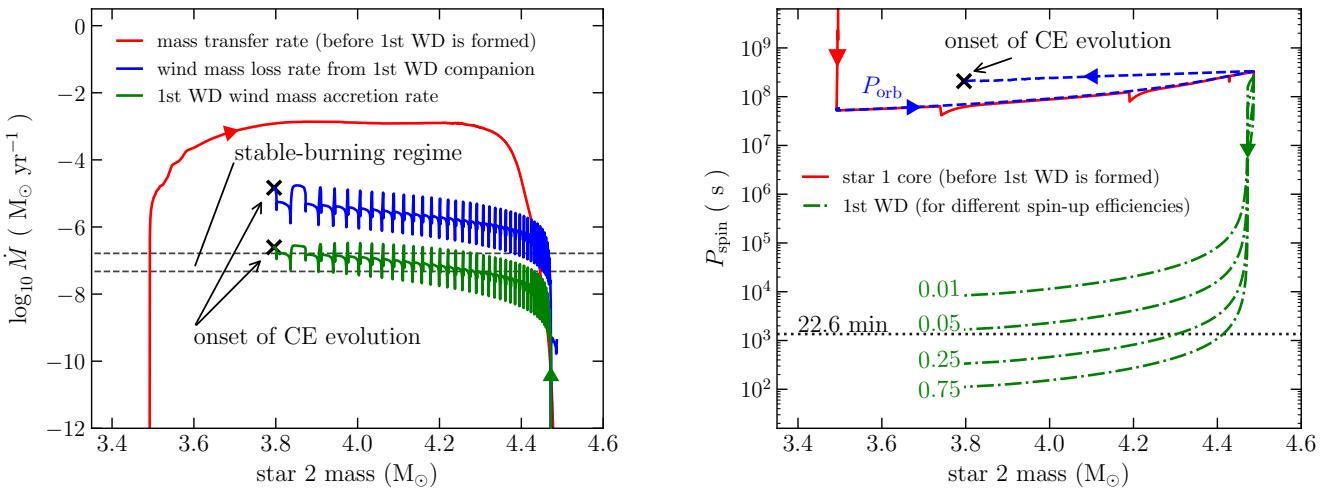

Figure 7.3: Evolution with the DA progenitor (star 2) mass of some properties of the best-fitting model for NLTT 12758, prior the onset of the common envelope phase, namely mass transfer rate during stable non-conservative mass transfer and wind mass-loss/accretion after the first white dwarf is formed (left-hand panel), and spin period of the DAP (first white dwarf) progenitor as well as of the DAP white dwarf (right-hand panel). The spin period of the DAP white dwarf is indicated as a dotted horizontal line in the right-hand panel. We reasonably well reproduce those properties in our modeling with the `MESA` code.

The good fit of the model to the observed binary suggests that the double white dwarf NLTT 12758, which hosts the only known magnetic white dwarf in such a system, did not form through two common envelope phases. This finding is in line with the results we obtained in previous chapters of this thesis. Two common envelope phases represent a poor model for reproducing the observed double white dwarf population.

Conclusion

The primary objective of this thesis was to compare two distinct methods for generating magnetic fields in binary white dwarfs. Astronomers have long observed white dwarf binaries due to their potential significance as detectable sources of gravitational waves and as a means to comprehend the origin of magnetic fields in white dwarfs. The formation of close double white dwarfs remains incompletely understood, and investigating the evolution of these systems offers a potential path to unravel the mysteries of their magnetic fields.

In pursuit of this goal, the Binary Stellar Evolution (`BSE`) code (Hurley et al., 2002b) was employed, and new codes were developed during this study to derive populations of binary white dwarfs suitable for analysis. Various combinations of parameters were explored to obtain diverse outputs, which were then used to scrutinize two different theories of evolution. We tested both formation theories using the formation channel of close double white dwarfs consisting of two common envelope phases.

As a first result, we find that the formation channel of two common envelopes does not reproduce the distribution of white dwarf masses of the observed systems. This clearly limits the constraints we can derive for theories on magnetic field generation.

Nevertheless, we tested the predictions of two scenarios for the generation of magnetic fields. The first postulated by Briggs et al. (2018) suggest that the magnetic field is generated during the common envelope phase, while the second developed by Schreiber et al. (2021b) following an idea of Isern et al. (2017b) attributes it to fast rotation and crystallization. In the former, as the giant star fills its Roche lobe, it engulfs the companion, and both cores enter a common envelope. Differential rotation within this envelope (or an accretion disk) leads to a strong magnetic field, which, upon ejection of the envelope, spreads through the vicinity of the degenerate hot core. The magnetic field freezes as the core cools and contracts. To study this theory, the equation proposed by Briggs et al. (2018) was utilized in this thesis. The second theory proposes a dynamo driven by fast rotation and a crystallized core, similar to those observed in low-mass stars or planets.

We find that the common envelope dynamo predicts a substantial number of systems with magnetic components, including for low-mass helium white dwarfs. This prediction drastically disagrees with the observations. The crystallization dynamo predictions are in general in somewhat

better agreement with the observations. Especially if we take into account that in most white dwarf binaries a magnetic field of the fainter component is difficult (if not impossible) to detect, and if we assume a small common envelope efficiency, the model predictions agree reasonably well with the observations.

In the observed sample of double white dwarfs, only one system with a magnetic companion is known. In line with the results described above, we suggest a formation scenario of this system that includes stable (non-conservative) mass transfer and the dynamo driven by fast rotation and crystallization. We found a very good solution describing the formation of this particular system.

For future work, we have in mind to improve this analysis using the stellar evolution code MESA which allows to properly simulate stable mass transfer.

Bibliography

Angel, J. R. P., Borra, E. F., and Landstreet, J. D. (1981). The magnetic fields of white dwarfs. *Astrophysical Journal, Supplement*, 45:457–474.

Bagnulo, S. and Landstreet, J. D. (2020). Discovery of six new strongly magnetic white dwarfs in the 20 pc local population. *Astronomy and Astrophysics*, 643:A134.

Bagnulo, S. and Landstreet, J. D. (2021a). New insight into the magnetism of degenerate stars from the analysis of a volume-limited sample of white dwarfs. *Monthly Notices of the Royal Astronomical Society*, 507(4):5902–5951.

Bagnulo, S. and Landstreet, J. D. (2021b). New insight into the magnetism of degenerate stars from the analysis of a volume limited sample of white dwarfs. *arXiv e-prints*, page arXiv:2106.11109.

Balbus, S. A. and Hawley, J. F. (1991). A Powerful Local Shear Instability in Weakly Magnetized Disks. I. Linear Analysis. *The Astrophysical Journal*, 376:214.

Bédard, A., Bergeron, P., Brassard, P., and Fontaine, G. (2020a). On the Spectral Evolution of Hot White Dwarf Stars. I. A Detailed Model Atmosphere Analysis of Hot White Dwarfs from SDSS DR12. *The Astrophysical Journal*, 901(2):93.

Bédard, A., Bergeron, P., Brassard, P., and Fontaine, G. (2020b). On the Spectral Evolution of Hot White Dwarf Stars. I. A Detailed Model Atmosphere Analysis of Hot White Dwarfs from SDSS DR12. *The Astrophysical Journal*, 901(2):93.

Belczynski, K., Kalogera, V., and Bulik, T. (2002). A Comprehensive Study of Binary Compact Objects as Gravitational Wave Sources: Evolutionary Channels, Rates, and Physical Properties. *The Astrophysical Journal*, 572(1):407–431.

Belloni, D. and Schreiber, M. R. (2020). Are white dwarf magnetic fields in close binaries generated during common-envelope evolution? *Monthly Notices of the Royal Astronomical Society*, 492(1):1523–1529.

Belloni, D. and Schreiber, M. R. (2023). Overall Binary Evolution Theory. *arXiv e-prints*, page arXiv:2303.08997.

Bergeron, P., Ruiz, M.-T., and Leggett, S. K. (1993). G62-46: an Unresolved Double Degenerate Binary Containing a Magnetic DA Component. *The Astrophysical Journal*, 407:733.

Bergeron, P., Saffer, R. A., and Liebert, J. (1992). A Spectroscopic Determination of the Mass Distribution of DA White Dwarfs. *The Astrophysical Journal*, 394:228.

Bergeron, P., Wesemael, F., Liebert, J., and Fontaine, G. (1989). Determination of the Atmospheric Parameters of the Binary DA White Dwarf L870-2 (EG 11). *The Astrophysical Journall*, 345:L91.

Bernasconi, P. A. and Maeder, A. (1996). About the absence of a proper zero age main sequence for massive stars. *Astronomy and Astrophysics*, 307:829–839.

Blackett, P. M. S. (1947). The Magnetic Field of Massive Rotating Bodies. *Nature Astronomy*, 159(4046):658–666.

Bloecker, T. (1995). Stellar evolution of low and intermediate-mass stars. I. Mass loss on the AGB and its consequences for stellar evolution. *Astronomy and Astrophysics*, 297:727.

Bours, M. C. P., Marsh, T. R., Gänsicke, B. T., Tauris, T. M., Istrate, A. G., Badenes, C., Dhillon, V. S., Gal-Yam, A., Hermes, J. J., Kengkriangkrai, S., Kilic, M., Koester, D., Mullally, F., Prasert, N., Steeghs, D., Thompson, S. E., and Thorstensen, J. R. (2015). A double white dwarf with a paradoxical origin? *Monthly Notices of the Royal Astronomical Society*, 450(4):3966–3974.

Bours, M. C. P., Marsh, T. R., Parsons, S. G., Copperwheat, C. M., Dhillon, V. S., Littlefair, S. P., Gänsicke, B. T., Gianninas, A., and Tremblay, P. E. (2014). Precise parameters for both white dwarfs in the eclipsing binary CSS 41177. *Monthly Notices of the Royal Astronomical Society*, 438(4):3399–3408.

Bragaglia, A., Greggio, L., Renzini, A., and D'Odorico, S. (1990). Double Degenerates among DA White Dwarfs. *The Astrophysical Journall*, 365:L13.

Braithwaite, J. and Spruit, H. C. (2004). A fossil origin for the magnetic field in A stars and white dwarfs. *Nature*, 431(7010):819–821.

Briggs, G. P., Ferrario, L., Tout, C. A., and Wickramasinghe, D. T. (2018). Genesis of magnetic fields in isolated white dwarfs. *Monthly Notices of the Royal Astronomical Society*, 478(1):899–905.

Brown, W. R., Kilic, M., Allende Prieto, C., Gianninas, A., and Kenyon, S. J. (2013). The ELM Survey. V. Merging Massive White Dwarf Binaries. *The Astrophysical Journal*, 769(1):66.

Brown, W. R., Kilic, M., Hermes, J. J., Allende Prieto, C., Kenyon, S. J., and Winget, D. E. (2011). A 12 Minute Orbital Period Detached White Dwarf Eclipsing Binary. *The Astrophysical Journall*, 737(1):L23.

Brown, W. R., Kilic, M., Kosakowski, A., Andrews, J. J., Heinke, C. O., Agüeros, M. A., Camilo, F., Gianninas, A., Hermes, J. J., and Kenyon, S. J. (2020a). The ELM Survey. VIII. Ninety-eight Double White Dwarf Binaries. *The Astrophysical Journal*, 889(1):49.

Brown, W. R., Kilic, M., Kosakowski, A., Andrews, J. J., Heinke, C. O., Agüeros, M. A., Camilo, F., Gianninas, A., Hermes, J. J., and Kenyon, S. J. (2020b). The ELM Survey. VIII. Ninety-eight Double White Dwarf Binaries. *The Astrophysical Journal*, 889(1):49.

Burdge, K. B., Coughlin, M. W., Fuller, J., Kaplan, D. L., Kulkarni, S. R., Marsh, T. R., Bellm, E. C., Dekany, R. G., Duev, D. A., Graham, M. J., Mahabal, A. A., Masci, F. J., Laher, R. R., Riddle, R., Soumagnac, M. T., and Prince, T. A. (2020). An 8.8 Minute Orbital Period Eclipsing Detached Double White Dwarf Binary. *The Astrophysical Journall*, 905(1):L7.

Burdge, K. B., Coughlin, M. W., Fuller, J., Kupfer, T., Bellm, E. C., Bildsten, L., Graham, M. J., Kaplan, D. L., Roestel, J. v., Dekany, R. G., Duev, D. A., Feeney, M., Giomi, M., Helou, G., Kaye, S., Laher, R. R., Mahabal, A. A., Masci, F. J., Riddle, R., Shupe, D. L., Soumagnac, M. T., Smith, R. M., Szkody, P., Walters, R., Kulkarni, S. R., and Prince, T. A. (2019). General relativistic orbital decay in a seven-minute-orbital-period eclipsing binary system. *Nature*, 571(7766):528–531.

Chandra, V., Hwang, H.-C., Zakamska, N. L., Gänsicke, B. T., Hermes, J. J., Schwope, A., Badenes, C., Tovmassian, G., Bauer, E. B., Maoz, D., Schreiber, M. R., Toloza, O. F., Inight, K. P., Rix, H.-W., and Brown, W. R. (2021). A 99 minute Double-lined White Dwarf Binary from SDSS-V. *The Astrophysical Journal*, 921(2):160.

Charbonnel, C. and Palacios, A. (2003). Rotating models for evolved low-mass stars. *arXiv e-prints*, pages astro–ph/0304518.

Christensen, U. R., Holzwarth, V., and Reiners, A. (2009). Energy flux determines magnetic field strength of planets and stars. *Nature*, 457(7226):167–169.

Coughlin, M. W., Burdge, K., Phinney, E. S., van Roestel, J., Bellm, E. C., Dekany, R. G., Delacroix, A., Duev, D. A., Feeney, M., Graham, M. J., Kulkarni, S. R., Kupfer, T., Laher,

R. R., Masci, F. J., Prince, T. A., Riddle, R., Rosnet, P., Smith, R., Serabyn, E., and Walters, R. (2020). ZTF J1901+5309: a 40.6-min orbital period eclipsing double white dwarf system. *Monthly Notices of the Royal Astronomical Society*, 494(1):L91–L96.

Davis, P. J., Kolb, U., and Willems, B. (2010). A comprehensive population synthesis study of post-common envelope binaries. *Monthly Notices of the Royal Astronomical Society*, 403(1):179–195.

Davis, P. J., Kolb, U., Willems, B., and Gänsicke, B. T. (2008). How many cataclysmic variables are crossing the period gap? A test for the disruption of magnetic braking. *Monthly Notices of the Royal Astronomical Society*, 389(4):1563–1576.

Dewi, J. D. M. and Tauris, T. M. (2000). On the energy equation and efficiency parameter of the common envelope evolution. *Astronomy and Astrophysics*, 360:1043–1051.

Dobbie, P. D., Baxter, R., Külebi, B., Parker, Q. A., Koester, D., Jordan, S., Lodieu, N., and Euchner, F. (2012). Two new young, wide, magnetic + non-magnetic double-degenerate binary systems. *Monthly Notices of the Royal Astronomical Society*, 421(1):202–212.

Ferrario, L., de Martino, D., and Gänsicke, B. T. (2015). Magnetic White Dwarfs. *Space Science Reviews*, 191(1-4):111–169.

Ferrario, L., Wickramasinghe, D., and Kawka, A. (2020). Magnetic fields in isolated and interacting white dwarfs. *Advances in Space Research*, 66(5):1025–1056.

García-Berro, E., Lorén-Aguilar, P., Aznar-Siguán, G., Torres, S., Camacho, J., Althaus, L. G., Córsico, A. H., Külebi, B., and Isern, J. (2012). Double Degenerate Mergers as Progenitors of High-field Magnetic White Dwarfs. *The Astrophysical Journal*, 749(1):25.

Ge, H., Hjellming, M. S., Webbink, R. F., Chen, X., and Han, Z. (2010). Adiabatic Mass Loss in Binary Stars. I. Computational Method. *The Astrophysical Journal*, 717(2):724–738.

Ge, H., Webbink, R. F., Chen, X., and Han, Z. (2015). Adiabatic Mass Loss in Binary Stars. II. From Zero-age Main Sequence to the Base of the Giant Branch. *The Astrophysical Journal*, 812(1):40.

Ge, H., Webbink, R. F., Chen, X., and Han, Z. (2020). Adiabatic Mass Loss in Binary Stars. III. From the Base of the Red Giant Branch to the Tip of the Asymptotic Giant Branch. *The Astrophysical Journal*, 899(2):132.

Gentile Fusillo, N. P., Tremblay, P.-E., Gänsicke, B. T., Manser, C. J., Cunningham, T., Cukanovaite, E., Hollands, M., Marsh, T., Raddi, R., Jordan, S., Toonen, S., Geier, S., Barstow, M., and Cummings, J. D. (2019). A Gaia Data Release 2 catalogue of white dwarfs and a comparison with SDSS. *Monthly Notices of the Royal Astronomical Society*, 482(4):4570–4591.

Ginzburg, S., Fuller, J., and Kawka, A. (2022). Slow convection and fast rotation in crystallization-driven white dwarf dynamos. *arXiv e-prints*, page arXiv:2202.12902.

Hallakoun, N., Maoz, D., Kilic, M., Mazeh, T., Gianninas, A., Agol, E., Bell, K. J., Bloemen, S., Brown, W. R., Debes, J., Faigler, S., Kull, I., Kupfer, T., Loeb, A., Morris, B. M., and Mullally, F. (2016). SDSS J1152+0248: an eclipsing double white dwarf from the Kepler K2 campaign. *Monthly Notices of the Royal Astronomical Society*, 458(1):845–854.

Han, Z., Podsiadlowski, P., and Eggleton, P. P. (1995a). The formation of bipolar planetary nebulae and close white dwarf binaries. *Monthly Notices of the Royal Astronomical Society*, 272(4):800–820.

Han, Z., Podsiadlowski, P., and Eggleton, P. P. (1995b). The formation of bipolar planetary nebulae and close white dwarf binaries. *Monthly Notices of the Royal Astronomical Society*, 272(4):800–820.

Holberg, J. B., Saffer, R. A., Tweedy, R. W., and Barstow, M. A. (1995). The Binary Double-degenerate Nature of the Bright DAO White Dwarf Feige 55. *The Astrophysical Journall*, 452:L133.

Hurley, J. R., Tout, C. A., and Pols, O. R. (2002a). Evolution of binary stars and the effect of tides on binary populations. *Monthly Notices of the Royal Astronomical Society*, 329(4):897–928.

Hurley, J. R., Tout, C. A., and Pols, O. R. (2002b). Evolution of binary stars and the effect of tides on binary populations. *Monthly Notices of the Royal Astronomical Society*, 329(4):897–928.

Iben, Icko, J. and Livio, M. (1993). Common Envelopes in Binary Star Evolution. *Publications of the Astronomical Society of the Pacific*, 105:1373.

Isern, J., García-Berro, E., Külebi, B., and Lorén-Aguilar, P. (2017a). A Common Origin of Magnetism from Planets to White Dwarfs. *The Astrophysical Journal*, 836(2):L28.

Isern, J., García-Berro, E., Külebi, B., and Lorén-Aguilar, P. (2017b). A Common Origin of Magnetism from Planets to White Dwarfs. 836(2):L28.

Isern, J., Mochkovitch, R., García-Berro, E., and Hernanz, M. (1997). The Physics of Crystallizing White Dwarfs. *The Astrophysical Journal*, 485(1):308–312.

Kaplan, D. L., Marsh, T. R., Walker, A. N., Bildsten, L., Bours, M. C. P., Breedt, E., Copperwheat, C. M., Dhillon, V. S., Howell, S. B., Littlefair, S. P., Shporer, A., and Steinfadt, J. D. R. (2014). Properties of an Eclipsing Double White Dwarf Binary NLTT 11748. *The Astrophysical Journal*, 780(2):167.

Kawka, A., Briggs, G. P., Vennes, S., Ferrario, L., Paunzen, E., and Wickramasinghe, D. T. (2017a). A fast spinning magnetic white dwarf in the double degenerate, super-Chandrasekhar system NLTT 12758. *Monthly Notices of the Royal Astronomical Society*, 466(1):1127–1139.

Kawka, A., Briggs, G. P., Vennes, S., Ferrario, L., Paunzen, E., and Wickramasinghe, D. T. (2017b). A fast spinning magnetic white dwarf in the double degenerate, super-Chandrasekhar system NLTT 12758. *Monthly Notices of the Royal Astronomical Society*, 466(1):1127–1139.

Kawka, A. and Vennes, S. (2004). Ap stars as progenitors of magnetic white dwarfs. In Zverko, J., Ziznovsky, J., Adelman, S. J., and Weiss, W. W., editors, *The A-Star Puzzle*, volume 224, pages 879–885.

Kemp, J. C., Swedlund, J. B., Landstreet, J. D., and Angel, J. R. P. (1970). Discovery of Circularly Polarized Light from a White Dwarf. *The Astrophysical Journal Letters*, 161:L77.

Kilic, M., Bédard, A., and Bergeron, P. (2021a). Hidden in plain sight: a double-lined white dwarf binary 26 pc away and a distant cousin. *Monthly Notices of the Royal Astronomical Society*, 502(4):4972–4980.

Kilic, M., Brown, W. R., Bédard, A., and Kosakowski, A. (2021b). The Discovery of Two LISA Sources within 0.5 kpc. *The Astrophysical Journall*, 918(1):L14.

Kilic, M., Hermes, J. J., Gianninas, A., Brown, W. R., Heinke, C. O., Agüeros, M. A., Chote, P., Sullivan, D. J., Bell, K. J., and Harrold, S. T. (2014). Found: the progenitors of AM CVn and supernovae .Ia. *Monthly Notices of the Royal Astronomical Society*, 438(1):L26–L30.

Koester, D., Voss, B., Napiwotzki, R., Christlieb, N., Homeier, D., Lisker, T., Reimers, D., and Heber, U. (2009). High-resolution UVES/VLT spectra of white dwarfs observed for the ESO SN Ia Progenitor Survey. III. DA white dwarfs. *Astronomy and Astrophysics*, 505(1):441–462.

Korol, V., Rossi, E. M., Groot, P. J., Nelemans, G., Toonen, S., and Brown, A. G. A. (2017). Prospects for detection of detached double white dwarf binaries with Gaia, LSST and LISA. *Monthly Notices of the Royal Astronomical Society*, 470(2):1894–1910.

Kroupa, P., Tout, C. A., and Gilmore, G. (1993). The Distribution of Low-Mass Stars in the Galactic Disc. *Monthly Notices of the Royal Astronomical Society*, 262:545–587.

Lagos, F., Schreiber, M. R., Zorotovic, M., Gänsicke, B. T., Ronco, M. P., and Hamers, A. S. (2021). WD 1856 b: a close giant planet around a white dwarf that could have survived a common envelope phase. *Monthly Notices of the Royal Astronomical Society*, 501(1):676–682.

Lamberts, A., Blunt, S., Littenberg, T. B., Garrison-Kimmel, S., Kupfer, T., and Sanderson, R. E. (2019). Predicting the LISA white dwarf binary population in the Milky Way with cosmological simulations. *Monthly Notices of the Royal Astronomical Society*, 490(4):5888–5903.

Landstreet, J. D. (2020). Reflections on the Discovery of the First Magnetic White Dwarf. In Wade, G., Alecian, E., Bohlender, D., and Sigut, A., editors, *Stellar Magnetism: A Workshop in Honour of the Career and Contributions of John D. Landstreet*, volume 11, pages 239–246.

Landstreet, J. D. and Bagnulo, S. (2020). Discovery of a Sirius-like binary system with a very strongly magnetic white dwarf. Binarity among magnetic white dwarfs. *Astronomy and Astrophysics*, 634:L10.

Liebert, J., Bergeron, P., and Holberg, J. B. (2005). The Formation Rate and Mass and Luminosity Functions of DA White Dwarfs from the Palomar Green Survey. *The Astrophysical Journal Supplement Series*, 156(1):47–68.

Liebert, J., Bergeron, P., Schmidt, G. D., and Saffer, R. A. (1993). Discovery of a Magnetic/Nonmagnetic Double-degenerate Binary System. *The Astrophysical Journal*, 418:426.

Lister, J. R. and Buffett, B. A. (1995). The strength and efficiency of thermal and compositional convection in the geodynamo. *Physics of the Earth and Planetary Interiors*, 91(1):17–30.

Livio, M. and Soker, N. (1988). The Common Envelope Phase in the Evolution of Binary Stars. *The Astrophysical Journal*, 329:764.

Marsh, T. R. (1995). The discovery of a short-period double-degenerate binary star. *Monthly Notices of the Royal Astronomical Society*, 275(1):L1–L5.

Marsh, T. R., Dhillon, V. S., and Duck, S. R. (1995a). Low-Mass White Dwarfs Need Friends - Five New Double-Degenerate Close Binary Stars. *Monthly Notices of the Royal Astronomical Society*, 275:828.

Marsh, T. R., Dhillon, V. S., and Duck, S. R. (1995b). Low-Mass White Dwarfs Need Friends - Five New Double-Degenerate Close Binary Stars. *Monthly Notices of the Royal Astronomical Society*, 275:828.

Marsh, T. R., Gänsicke, B. T., Hümmerich, S., Hambsch, F. J., Bernhard, K., Lloyd, C., Breedt, E., Stanway, E. R., Steeghs, D. T., Parsons, S. G., Toloza, O., Schreiber, M. R., Jonker, P. G., van Roestel, J., Kupfer, T., Pala, A. F., Dhillon, V. S., Hardy, L. K., Littlefair, S. P., Aungwerojwit, A., Arjyotha, S., Koester, D., Bochinski, J. J., Haswell, C. A., Frank, P., and Wheatley, P. J. (2016). A radio-pulsing white dwarf binary star. *Nature Astronomy*, 537(7620):374–377.

Matthews, K., Nakajima, T., Kulkarni, S., and Oppenheimer, B. (1995). Gliese 229B. *IAU Circulars*, 6280:2.

Maxted, P. F. L., Burleigh, M. R., Marsh, T. R., and Bannister, N. P. (2002a). PG 1115+166 - a long-period DA+DB binary. *Monthly Notices of the Royal Astronomical Society*, 334(4):833–839.

Maxted, P. F. L. and Marsh, T. R. (1999). The fraction of double degenerates among DA white dwarfs. *Monthly Notices of the Royal Astronomical Society*, 307(1):122–132.

Maxted, P. F. L., Marsh, T. R., and Moran, C. K. J. (2002b). The mass ratio distribution of short-period double degenerate stars. *Monthly Notices of the Royal Astronomical Society*, 332(3):745–753.

Maxted, P. F. L., Marsh, T. R., Moran, C. K. J., and Han, Z. (2000). The triple degenerate star WD 1704+481. *Monthly Notices of the Royal Astronomical Society*, 314(2):334–337.

Morales-Rueda, L., Marsh, T. R., Maxted, P. F. L., Nelemans, G., Karl, C., Napiwotzki, R., and Moran, C. K. J. (2005). Six detached white-dwarf close binaries. *Monthly Notices of the Royal Astronomical Society*, 359(2):648–662.

Moran, C., Marsh, T. R., and Bragaglia, A. (1997). A detached double degenerate with a 1.4-h orbital period. *Monthly Notices of the Royal Astronomical Society*, 288(2):538–544.

Mullally, F., Badenes, C., Thompson, S. E., and Lupton, R. (2009). Twins: The Two Shortest Period Non-Interacting Double Degenerate White Dwarf Stars. *The Astrophysical Journall*, 707(1):L51–L55.

Napiwotzki, R., Karl, C. A., Lisker, T., Catalán, S., Drechsel, H., Heber, U., Homeier, D., Koester, D., Leibundgut, B., Marsh, T. R., Moehler, S., Nelemans, G., Reimers, D., Renzini, A., Ströer, A., and Yungelson, L. (2020). The ESO supernovae type Ia progenitor survey (SPY). The radial velocities of 643 DA white dwarfs. *Astronomy and Astrophysics*, 638:A131.

Nelan, E. P. (2007). Resolving LB 11146 with Hubble Space Telescope's Fine Guidance Sensor. *The Astrophysical Journal*, 134(5):1934–1937.

Nelemans, G., Napiwotzki, R., Karl, C., Marsh, T. R., Voss, B., Roelofs, G., Izzard, R. G., Montgomery, M., Reerink, T., Christlieb, N., and Reimers, D. (2005). Binaries discovered by the SPYproject. IV. Five single-lined DA double white dwarfs. *Astronomy and Astrophysics*, 440(3):1087–1095.

Nelemans, G., Yungelson, L. R., Portegies Zwart, S. F., and Verbunt, F. (2001). Population synthesis for double white dwarfs . I. Close detached systems. *Astronomy & Astrophysics*, 365:491–507.

Nordhaus, J., Wellons, S., Spiegel, D. S., Metzger, B. D., and Blackman, E. G. (2011). Formation of high-field magnetic white dwarfs from common envelopes. *Proceedings of the National Academy of Science*, 108(8):3135–3140.

Paczynski, B. (1976). Common Envelope Binaries. In Eggleton, P., Mitton, S., and Whelan, J., editors, *Structure and Evolution of Close Binary Systems*, volume 73, page 75.

Pala, A. F., Gänsicke, B. T., Breedt, E., Knigge, C., Hermes, J. J., Gentile Fusillo, N. P., Hollands, M. A., Naylor, T., Pelisoli, I., Schreiber, M. R., Toonen, S., Aungwerojwit, A., Cukanovaite, E., Dennihy, E., Manser, C. J., Pretorius, M. L., Scaringi, S., and Toloza, O. (2020). A Volume-limited Sample of Cataclysmic Variables from Gaia DR2: Space Density and Population Properties. *Monthly Notices of the Royal Astronomical Society*, 494(3):3799–3827.

Palla, F. (2012). 1961-2011: Fifty years of Hayashi tracks. In Umemura, M. and Omukai, K., editors, *First Stars IV - from Hayashi to the Future* -, volume 1480 of *American Institute of Physics Conference Series*, pages 22–29.

Parsons, S. G., Brown, A. J., Littlefair, S. P., Dhillon, V. S., Marsh, T. R., Hermes, J. J., Istrate, A. G., Breedt, E., Dyer, M. J., Green, M. J., and Sahman, D. I. (2020). A pulsating white dwarf in an eclipsing binary. *Nature Astronomy*, 4:690–696.

Parsons, S. G., Gänsicke, B. T., Schreiber, M. R., Marsh, T. R., Ashley, R. P., Breedt, E., Littlefair, S. P., and Meusinger, H. (2021a). Magnetic white dwarfs in post-common-envelope binaries. *Monthly Notices of the Royal Astronomical Society*, 502(3):4305–4327.

Parsons, S. G., Gänsicke, B. T., Schreiber, M. R., Marsh, T. R., Ashley, R. P., Breedt, E., Littlefair, S. P., and Meusinger, H. (2021b). Magnetic white dwarfs in post-common-envelope binaries. *Monthly Notices of the Royal Astronomical Society*, 502(3):4305–4327.

Parsons, S. G., Marsh, T. R., Gänsicke, B. T., Drake, A. J., and Koester, D. (2011). A Deeply Eclipsing Detached Double Helium White Dwarf Binary. *The Astrophysical Journall*, 735(2):L30.

Rebassa-Mansergas, A., Parsons, S. G., García-Berro, E., Gänsicke, B. T., Schreiber, M. R., Rybicka, M., and Koester, D. (2017). Orbital periods and component masses of three double white dwarfs. *Monthly Notices of the Royal Astronomical Society*, 466(2):1575–1581.

Regős, E. and Tout, C. A. (1995). The effect of magnetic fields in common-envelope evolution on the formation of cataclysmic variables. *Monthly Notices of the Royal Astronomical Society*, 273(1):146–156.

Reid, I. N., Liebert, J., and Schmidt, G. D. (2001). Discovery of a Magnetic DZ White Dwarf with Zeeman-Split Lines of Heavy Elements. *The Astrophysical Journal Letter*, 550(1):L61–L63.

Ruiter, A. J., Belczynski, K., Benacquista, M., Larson, S. L., and Williams, G. (2010). The LISA Gravitational Wave Foreground: A Study of Double White Dwarfs. *The Astrophysical Journal*, 717(2):1006–1021.

Saffer, R. A., Liebert, J., and Olszewski, E. W. (1988). Discovery of a Close Detached Binary DA White Dwarf System. *The Astrophysical Journal*, 334:947.

Salaris, M. and Cassisi, S. (2005). *Evolution of Stars and Stellar Populations*.

Salaris, M., Cassisi, S., Pietrinferni, A., Kowalski, P. M., and Isern, J. (2010a). A Large Stellar Evolution Database for Population Synthesis Studies. VI. White Dwarf Cooling Sequences. *The Astrophysical Journal*, 716(2):1241–1251.

Salaris, M., Cassisi, S., Pietrinferni, A., Kowalski, P. M., and Isern, J. (2010b). A Large Stellar Evolution Database for Population Synthesis Studies. VI. White Dwarf Cooling Sequences. *The Astrophysical Journal*, 716(2):1241–1251.

Saumon, D., Blouin, S., and Tremblay, P.-E. (2022). Current challenges in the physics of white dwarf stars. *Physics Reports*, 988:1–63.

Schaller, G., Schaerer, D., Meynet, G., and Maeder, A. (1992). New Grids of Stellar Models from 0.8-SOLAR-MASS to 120-SOLAR-MASSES at Z=0.020 and Z=0.001. *Astronomy and Astrophysics, Supplement*, 96:269.

Schenker, K. and King, A. R. (2002). A new evolutionary picture for CVs and LMXBs. II. The impact of thermal-timescale mass transfer. In Gänsicke, B. T., Beuermann, K., and Reinsch, K., editors, *The Physics of Cataclysmic Variables and Related Objects*, volume 261 of *Astronomical Society of the Pacific Conference Series*, page 242.

Schmidt, G. D., Harris, H. C., Liebert, J., Eisenstein, D. J., Anderson, S. F., Brinkmann, J., Hall, P. B., Harvanek, M., Hawley, S., Kleinman, S. J., Knapp, G. R., Krzesinski, J., Lamb, D. Q., Long, D., Munn, J. A., Neilsen, E. H., Newman, P. R., Nitta, A., Schlegel, D. J., Schneider, D. P., Silvestri, N. M., Smith, J. A., Snedden, S. A., Szkody, P., and Vanden Berk, D. (2003). Magnetic White Dwarfs from the Sloan Digital Sky Survey: The First Data Release. *The Astrophysical Journal*, 595(2):1101–1113.

Schreiber, M. R., Belloni, D., Gänsicke, B. T., Parsons, S. G., and Zorotovic, M. (2021a). The origin and evolution of magnetic white dwarfs in close binary stars. *Nature Astronomy*, 5:648–654.

Schreiber, M. R., Belloni, D., Gänsicke, B. T., Parsons, S. G., and Zorotovic, M. (2021b). The origin and evolution of magnetic white dwarfs in close binary stars. *Nature Astronomy*, 5:648–654.

Schreiber, M. R., Belloni, D., Zorotovic, M., Zapata, S., Gänsicke, B. T., and Parsons, S. G. (2022). Magnetic dynamos in white dwarfs - III. Explaining the occurrence of strong magnetic fields in close double white dwarfs. *Monthly Notices of the Royal Astronomical Society*, 513(2):3090–3103.

Schrinner, M. and Deinzer, W. (2001). On the post main sequence expansion of stars with contracting helium cores. *Astronomy and Astrophysics*, 379:496–500.

Sen, K., Langer, N., Marchant, P., Menon, A., de Mink, S. E., Schootemeijer, A., Schürmann, C., Mahy, L., Hastings, B., Nathaniel, K., Sana, H., Wang, C., and Xu, X. T. (2022). Detailed models of interacting short-period massive binary stars. *Astronomy and Astrophysics*, 659:A98.

Soberman, G. E., Phinney, E. S., and van den Heuvel, E. P. J. (1997). Stability criteria for mass transfer in binary stellar evolution. *Astronomy and Astrophysics*, 327:620–635.

Soker, N. (2002). Why every bipolar planetary nebula is 'unique'. *Monthly Notices of the Royal Astronomical Society*, 330(2):481–486.

Somers, G. and Pinsonneault, M. H. (2015). Older and colder: The impact of starspots on pre-main-sequence stellar evolution. *The Astrophysical Journal*, 807(2):174.

Steinfadt, J. D. R., Kaplan, D. L., Shporer, A., Bildsten, L., and Howell, S. B. (2010). Discovery of the Eclipsing Detached Double White Dwarf Binary NLTT 11748. *The Astrophysical Journall*, 716(2):L146–L151.

Toonen, S., Nelemans, G., and Portegies Zwart, S. (2012). Supernova Type Ia progenitors from merging double white dwarfs. Using a new population synthesis model. *Astronomy and Astrophysics*, 546:A70.

Tout, C. A., Wickramasinghe, D. T., Liebert, J., Ferrario, L., and Pringle, J. E. (2008). Binary star origin of high field magnetic white dwarfs. *Monthly Notices of the Royal Astronomical Society*, 387(2):897–901.

Tremblay, P. E., Hollands, M. A., Gentile Fusillo, N. P., McCleery, J., Izquierdo, P., Gänsicke, B. T., Cukanovaite, E., Koester, D., Brown, W. R., Charpinet, S., Cunningham, T., Farihi, J., Giammichele, N., van Grootel, V., Hermes, J. J., Hoskin, M. J., Jordan, S., Kepler, S. O., Kleinman, S. J., Manser, C. J., Marsh, T. R., de Martino, D., Nitta, A., Parsons, S. G., Pelisoli, I., Raddi, R., Rebassa-Mansergas, A., Ren, J. J., Schreiber, M. R., Silvotti, R., Toloza, O., Toonen, S., and Torres, S. (2020). Gaia white dwarfs within 40 pc - I. Spectroscopic observations of new candidates. *Monthly Notices of the Royal Astronomical Society*, 497(1):130–145.

van Horn, H. M. (1984). The Physics of White Dwarfs. In *Astrophysics Today*, page 129.

van Oirschot, P., Nelemans, G., Toonen, S., Pols, O., Brown, A. G. A., Helmi, A., and Portegies Zwart, S. (2014). Binary white dwarfs in the halo of the Milky Way. *Astronomy & Astrophysics*, 569:A42.

Vennes, S., Kawka, A., Vaccaro, T. R., and Silvestri, N. M. (2009). The double degenerate LP 400-22 revisited. *Astronomy and Astrophysics*, 507(3):1613–1616.

Vennes, S., Thorstensen, J. R., Kawka, A., Németh, P., Skinner, J. N., Pigulski, A., Ste&şacute, licki, M., Kołaczkowski, Z., and Śródka, P. (2011). Discovery of a Bright, Extremely Low Mass White Dwarf in a Close Double Degenerate System. *The Astrophysical Journall*, 737(1):L16.

Wesemael, F., Bergeron, P., Lamontagne, R. L., Fontaine, G., Beauchamp, A., Demers, S., Irwin, M. J., Holberg, J. B., Kepler, S. O., and Vennes, S. (1994). Hot Degenerates in the Montreal-Cambridge-Tololo Survey. II. Two New Hybrid White Dwarfs, MCT 0128-3846 and MCT 0453-2933, and the Nature of the DAB Stars. *The Astrophysical Journal*, 429:369.

Wheeler, J. C. (2012). White Dwarf/M Dwarf Binaries as Single Degenerate Progenitors of Type Ia Supernovae. *The Astrophysical Journal*, 758(2):123.

Wickramasinghe, D. T. and Ferrario, L. (2005). The origin of the magnetic fields in white dwarfs. *Monthly Notices of the Royal Astronomical Society*, 356(4):1576–1582.

Wijnen, T. P. G., Zorotovic, M., and Schreiber, M. R. (2015). White dwarf masses in cataclysmic variables. *Astronomy and Astrophysics*, 577:A143.

Zorotovic, M., Schreiber, M. R., Gänsicke, B. T., and Nebot Gómez-Morán, A. (2010). Post-common-envelope binaries from SDSS. IX: Constraining the common-envelope efficiency. *Astronomy and Astrophysics*, 520:A86.

Zorotovic, M., Schreiber, M. R., García-Berro, E., Camacho, J., Torres, S., Rebassa-Mansergas, A., and Gänsicke, B. T. (2014a). Monte Carlo simulations of post-common-envelope white dwarf + main sequence binaries: The effects of including recombination energy. *Astronomy & Astrophysics*, 568:A68.

Zorotovic, M., Schreiber, M. R., and Parsons, S. G. (2014b). The evolution of the self-lensing binary KOI-3278: evidence of extra energy sources during CE evolution. *Astronomy and Astrophysics*, 568:L9.